ACS Infectious Diseases

Article

pubs.acs.org/journal/aidcbc

Bedaquiline and Pyrazinamide Treatment Responses Are Affected by Pulmonary Lesion Heterogeneity in *Mycobacterium tuberculosis* Infected C3HeB/FeJ Mice

Scott M. Irwin,[†] Brendan Prideaux,[‡] Edward R. Lyon,[†] Matthew D. Zimmerman,[‡] Elizabeth J. Brooks,[†] Christopher A. Schrupp,[†] Chao Chen,[‡] Matthew J. Reichlen,[§] Bryce C. Asay,[†] Martin I. Voskuil,[§] Eric L. Nuermberger,[∥] Koen Andries,[⊥] Michael A. Lyons,[†] Véronique Dartois,[‡] and Anne J. Lenaerts*[,†]

[†]Mycobacteria Research Laboratories, Department of Microbiology, Immunology and Pathology, Colorado State University, Fort Collins, Colorado 80523, United States

[‡]Public Health Research Institute, New Jersey Medical School, Rutgers, The State University of New Jersey, Newark, New Jersey 07103, United States

[§]Department of Immunology and Microbiology, University of Colorado School of Medicine, Aurora, Colorado 80045, United States

[∥]Center for Tuberculosis Research, Department of Medicine, Johns Hopkins University School of Medicine, Baltimore, Maryland 21231, United States

[⊥]Department of Infectious Diseases, Janssen Pharmaceutica, 2340 Beerse, Belgium

Supporting Information

ABSTRACT: BALB/c and Swiss mice are routinely used to validate the effectiveness of tuberculosis drug regimens, although these mouse strains fail to develop human-like pulmonary granulomas exhibiting caseous necrosis. Microenvironmental conditions within human granulomas may negatively impact drug efficacy, and this may not be reflected in non-necrotizing lesions found within conventional mouse models. The C3HeB/FeJ mouse model has been increasingly utilized as it develops hypoxic, caseous necrotic granulomas which may more closely mimic the pathophysiological conditions found within human pulmonary granulomas. Here, we examined the treatment response of BALB/c and C3HeB/FeJ mice to bedaquiline (BDQ) and pyrazinamide (PZA) administered singly and in combination. BALB/c mice consistently displayed a highly uniform treatment response to both drugs, while C3HeB/FeJ mice displayed a bimodal response composed of responsive and less-responsive mice. Plasma pharmacokinetic analysis of dissected lesions from BALB/c and C3HeB/FeJ mice revealed that PZA penetrated lesion types from both mouse strains with similar efficiency. However, the pH of the necrotic caseum of C3HeB/FeJ granulomas was determined to be 7.5, which is in the range where PZA is essentially ineffective under standard laboratory in vitro growth conditions. BDQ preferentially accumulated within the highly cellular regions in the lungs of both mouse strains, although it was present at reduced but still biologically relevant concentrations within the central caseum when dosed at 25 mg/kg. The differential treatment response which resulted from the heterogeneous pulmonary pathology in the C3HeB/FeJ mouse model revealed several factors which may impact treatment efficacy, and could be further evaluated in clinical trials.

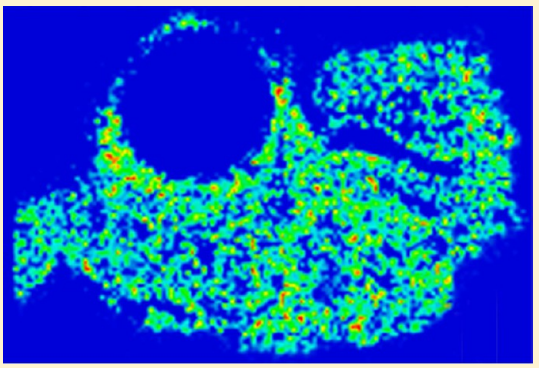

KEYWORDS: *C3HeB/FeJ, mouse models, bedaquiline, pyrazinamide, tuberculosis*

Preclinical animal models that aim to accurately reflect the pulmonary pathology observed during human disease are an essential component of tuberculosis (TB) drug development programs. Humans infected with *Mycobacterium tuberculosis* generally develop multiple histologically distinct lesion types within the lungs following infection.[1,2] The progression of disease within the lungs resulting in this lesion heterogeneity is both a complex and dynamic process. One particular lesion type is characterized by a central region of caseous necrosis encapsulated by collagen, which is believed to contain the bacilli and prevent dissemination to other organs of the body. The primary drawback of standard mouse models is that they fail to replicate the caseous necrotic pathology that is the hallmark of disease in humans. The impact that the intralesional environment can have on drug penetration and drug responsiveness of metabolically distinct bacterial subpopulations has been an important but neglected area of research.[3,4]

C3HeB/FeJ mice are increasingly being utilized as an animal model for TB drug development due to the formation of highly

Received: October 26, 2015
Published: February 24, 2016

DOI: 10.1021/acsinfecdis.5b00127
ACS Infect. Dis. 2016, 2, 251−267

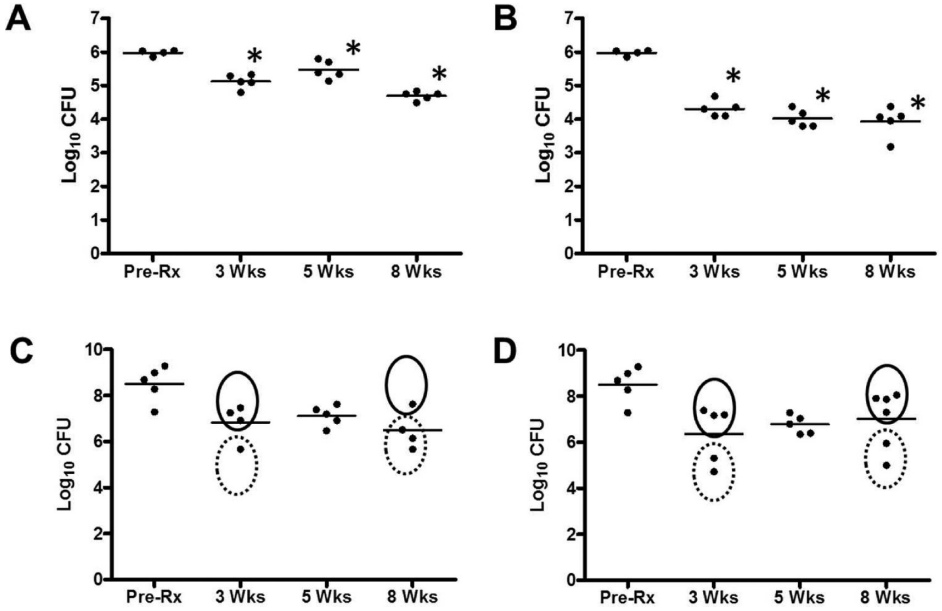

Figure 1. PZA activity in BALB/c and C3HeB/FeJ mice. Plots represent $\log_{10}$ CFU determinations from the lungs of individual BALB/c (A, B) or C3HeB/FeJ (C, D) mice. Eight weeks following LDA infection, mice were treated for 3, 5, or 8 weeks with 150 (A, C) or 300 mg/kg (B, D) PZA via oral gavage. Pre-Rx represents untreated mice aerosol infected for 8 weeks. Ovals with solid lines represent the PZA less-responsive subpopulation, and dashed lines represent the PZA responsive subpopulation of C3HeB/FeJ mice. Pre-Rx and defined time points were determined to be statistically different (*; $P < 0.01$) using a one-way ANOVA. Responsive and less-responsive populations were determined to be statistically different ($P < 0.001$) using a two-way ANOVA.

organized, caseous necrotic pulmonary granulomas following low dose aerosol (LDA) infection with *M. tuberculosis*.[5] These granulomas more closely resemble those found in TB patients compared to the standard laboratory mouse strains. A recent report from our laboratory identified that C3HeB/FeJ mice respond to LDA infection with *M. tuberculosis* Erdman by developing three morphologically distinct pulmonary lesion types.[1,6] In contrast, BALB/c mice only present with a single lesion type. The spectrum of lesion types in C3HeB/FeJ mice consists of highly encapsulated caseous necrotic granulomas (type I), fulminant neutrophilic alveolitis (type II), and cellular non-necrotizing lesions (type III), with only the latter lesion type being present in BALB/c mice. Importantly, these lesion types exhibit highly different microenvironmental conditions that vary in certain parameters such as oxygen tension, pH, nutrient supply, and cellular composition which can have profound effects on drug efficacy. In support of this, it has been shown that the activity of clofazimine (CFZ) is highly attenuated in C3HeB/FeJ mice possessing hypoxic caseous necrotic granulomas when compared to BALB/c mice showing only cellular non-necrotizing lesions that fail to become hypoxic.[7] However, the activity of CFZ could be reconstituted in C3HeB/FeJ mice when CFZ was given prior to the formation of caseous necrotic granulomas. In this earlier report, we also described a series of in vitro assays where CFZ activity strongly correlated with the level of aeration of an in vitro *M. tuberculosis* culture. The observation that CFZ activity appears tightly linked to oxygen levels is in concordance with results described by Rubin et al., which suggests CFZ can siphon off electrons from NDH-2.[8] Furthermore, Lanoix et al. identified a divergent treatment response in C3HeB/FeJ mice following treatment with pyrazinamide (PZA), and suggested that the relatively neutral pH within caseous necrotic granulomas (pH 7.4) likely accounted for the lack of efficacy although drug penetration into caseous necrotic granulomas was not directly examined in this study.[9] Taken together, these results highlight the impact that localized lesion environmental conditions have upon drug efficacy within the lung, which underscores the importance of choosing preclinical animal models that reflect the complex pathological response present in humans with TB.[7,9]

The diarylquinoline bedaquiline (BDQ; Sirturo, TMC207) is the first TB drug to be approved by the Food and Drug Administration in over 40 years. BDQ has been shown to be highly active against both actively replicating and nonreplicating bacterial subpopulations.[10] It also exhibits significant efficacy in preclinical animal models[11,12] as well as in patients infected with multidrug resistant TB.[13,14] In order to prevent the emergence of drug resistance and to maximize the efficacy of this potent new drug, careful consideration should be given to combination regimen design and implementation.

PZA is a critical drug in the TB arsenal which played an essential role in shortening the standard treatment regimen from nine to six months.[15,16] It often displays significant synergy with novel and existing TB drugs in preclinical animal models as well as human early bactericidal activity studies.[17−19] Although its mechanism of action is not precisely known, it has been suggested that PZA may act as an uncoupler affecting membrane potential,[20] may inhibit trans-translation,[21] and/or may target *panD* involved in pantothenate biosynthesis.[22] Early studies using intravenous infection of Swiss mice demonstrated that BDQ and PZA combination therapy had bactericidal activity superior to the standard first-line regimen as well as synergistic activity during the sterilizing phase.[11,18] Using the more realistic LDA infection model showed that treatment with BDQ and PZA could prevent relapse in 100% of BALB/c mice treated for 3 months, demonstrating the remarkable treatment-shortening potential of this highly potent combination.[23] Based on their considerable synergism, drug regimens containing both BDQ and PZA are being considered by the Global Alliance for

DOI: 10.1021/acsinfecdis.5b00127
ACS Infect. Dis. 2016, 2, 251−267

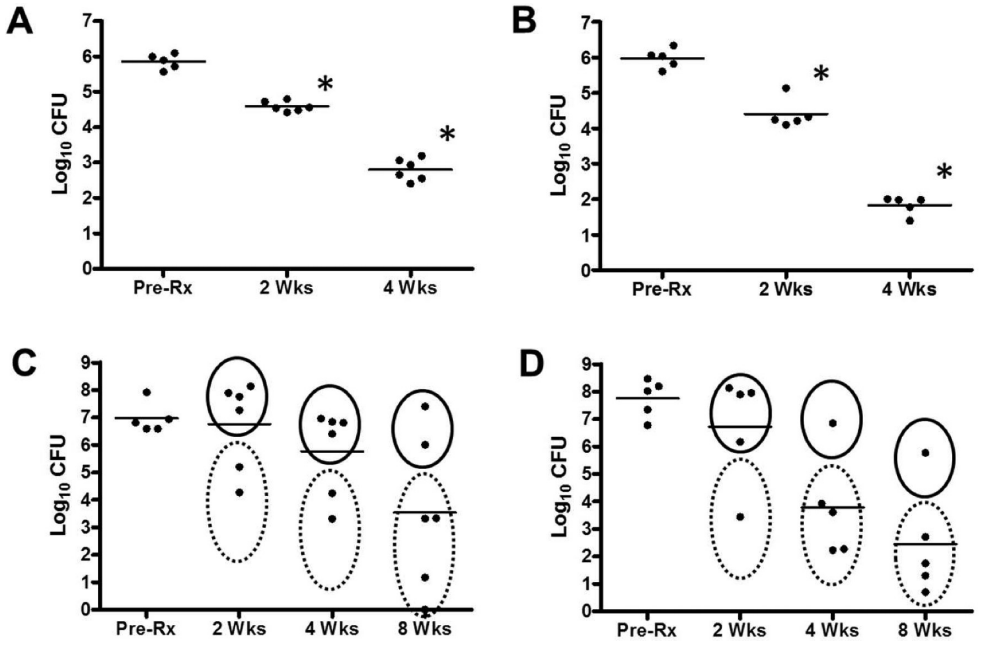

Figure 2. BDQ exhibited dose-dependent activity between 10 and 25 mg/kg. Plots represent $\log_{10}$ CFU determinations from the lungs of individual BALB/c (A, B) or C3HeB/FeJ (C, D) mice. Eight weeks following LDA infection, mice were treated with BDQ 10 mg/kg (A, C) or 25 mg/kg (B, D) via oral gavage. BALB/c mice were treated for either 2 or 4 weeks. C3HeB/FeJ mice were treated for either 2, 4, or 8 weeks. Pre-Rx represents untreated mice aerosol infected for 8 weeks. Ovals with solid lines represent the BDQ less-responsive subpopulation, and dashed lines represent the BDQ responsive subpopulation of C3HeB/FeJ mice. Pre-Rx and defined time points were determined to be statistically different (*; $P < 0.01$) using a one-way ANOVA. Responsive and less-responsive populations were determined to be statistically different ($P < 0.001$) using a two-way ANOVA.

TB Drug Development as a critical component of treatment-shortening regimens in clinical trials.[24]

Although the bactericidal and sterilizing activity of BDQ and PZA combination therapy has been convincingly demonstrated in BALB/c and Swiss mice, studies have not been performed in small animal models that replicate the caseous necrotic pulmonary pathology more closely resembling that seen in TB patients. In these experiments, we compared the treatment response of BALB/c and C3HeB/FeJ mice using BDQ and PZA, both singly and in combination, to determine whether differences in the pulmonary pathology impact the efficacy of these two synergistic TB drugs. A comprehensive plasma, lung, and lesion-specific PK analysis was also performed to characterize drug exposure and accumulation within pulmonary tissues. This information was used in conjunction with matrix-assisted laser desorption/ionization mass spectrometry imaging (MALDI-MSI) to more precisely characterize drug distribution and accumulation within specific lesion types over time.

Part of the results presented here has been presented at the Keystone Symposium on Host Response in Tuberculosis (Abstract # 1076, Santa Fe, NM, January 2015).

RESULTS AND DISCUSSION

Activity of PZA in BALB/c and C3HeB/FeJ Mice. BALB/c and C3HeB/FeJ mice infected with *M. tuberculosis* Erdman were treated with a standard PZA dose of 150 mg/kg, or a higher dose of 300 mg/kg. In both strains of mice, during the first 3 weeks of treatment with 150 mg/kg PZA there was a significant decrease in pulmonary CFU (Figures 1A and 1C; $P < 0.01$). Treatment with 300 mg/kg PZA resulted in a larger decrease in CFU (Figures 1B and 1D; $P < 0.01$), indicating a dose-dependent response within the first 3 weeks. However, even at 300 mg/kg, continuation of PZA treatment for another 2 or 5 weeks did not confer additional protection ($P > 0.05$). Interanimal treatment response in BALB/c mice was highly uniform, while in C3HeB/FeJ mice, treatment response was more heterogeneous with a substantially larger interanimal variation (encompassing approximately 3 orders of magnitude of variation within the same treatment group). While the variation in treatment response of BALB/c mice was unimodal, the variation observed in C3HeB/FeJ mice was determined to be a bimodal distribution composed of "responsive" and "less-responsive" mouse subpopulations. The two treatment responses in C3HeB/FeJ mice were found to be significantly different ($P < 0.001$) when the bacterial load in lungs was compared using a two-way ANOVA statistical test. Thus, PZA treatment revealed a bimodal treatment response in C3HeB/FeJ mice which display more realistic pulmonary pathology in contrast to the unimodal treatment response observed in BALB/c mice.

Due to the sensitivity of PZA to pH, we next measured the pH of dissected caseum samples. For three individual samples, the pH values were 7.4, 7.6, and 7.6. These values were similar to results recently published using C3HeB/FeJ mice aerosol infected with *M. tuberculosis* H37Rv strain.[9] At this pH, the MIC of PZA is elevated to a level typically not achievable in vivo.[25]

Activity of BDQ in BALB/c and C3HeB/FeJ Mice. In this experiment, mice were treated with either a low dose (10 mg/kg) or a standard dose (25 mg/kg) of BDQ to determine efficacy in BALB/c and C3HeB/FeJ mice. The rationale for selecting the low BDQ dose was to avoid masking the efficacy of PZA when the drugs were used together due to the highly potent activity of BDQ. In BALB/c mice, BDQ was highly effective and showed increased activity over time culminating in a 3.1 $\log_{10}$ CFU reduction following 4 weeks of treatment with 10 mg/kg (Figure 2A) and a 4.1 $\log_{10}$ CFU reduction using 25 mg/kg (Figure 2B). The treatment response to BDQ was also

DOI: 10.1021/acsinfecdis.5b00127
ACS Infect. Dis. 2016, 2, 251−267

very uniform across all mice, with minimal variation in pulmonary bacterial counts between replicate mice.

In contrast to BALB/c mice, C3HeB/FeJ mice displayed far greater variation in log transformed pulmonary bacterial counts (encompassing a range of about 5−6 orders of magnitude within the same treatment group). Further analysis revealed that, for both 10 and 25 mg/kg doses, a bimodal distribution in treatment response was evident in C3HeB/FeJ mice that was not observed in BALB/c mice (Figures 2C and 2D), whereby one group of mice was responsive to the drug and the other showed reduced activity after BDQ treatment. The treatment response of the responsive and less-responsive mouse subpopulations of C3HeB/FeJ mice was found to be significantly different ($P < 0.001$) using a two-way ANOVA statistical test. Although statistical comparisons were limited by division of the mice into two groups, a trend appeared when comparing the results of the higher dose treatment groups with the lower dose. The dose range effect was reflected in two ways. First, more mice were present in the responding subpopulation at the standard 25 mg/kg dose of BDQ when compared to the 10 mg/kg group (indicated by the mouse numbers within the ovals with dashed lines in Figures 2C and 2D). In the less-responsive subpopulation, 10 mg/kg BDQ was only bacteriostatic while 25 mg/kg appeared to have increased efficacy against this subpopulation (indicated by the mouse numbers within the ovals with solid lines in Figure 2D). Second, not only was the number of less-responsive mice lower for the 25 mg/kg groups versus the 10 mg/kg, the results also suggested that only BDQ at 25 mg/kg showed activity against bacteria in all mice. In order to quantify this, the results were analyzed by studying the rate of reduction in bacterial load of the less-responsive mouse population. For this purpose, the rate of $\log_{10}$ CFU reduction from 4 to 8 weeks of treatment was calculated from the mean mouse subpopulation values (Table 1). The

Table 1. BDQ/PZA Combination Therapy Has Increased Efficacy Primarily against the Less-Responsive C3HeB/FeJ Mouse Subpopulation[a]

treatment (mg/kg)	less-responsive	responsive
BDQ (10)	0.0129	0.4392
BDQ (25)	0.2783	0.3606
BDQ/PZA (10/150)	0.2962	0.2178

[a]Numbers represent the rate of decrease in $\log_{10}$ CFU in the lungs between 4 and 8 weeks of treatment. The rate was calculated as the amount of CFU reduction over the time interval (in weeks), as represented by $-(\Delta\log_{10}\text{ CFU})/\Delta t$.

calculations showed that treatment with 10 mg/kg BDQ resulted in a slower rate of decrease in CFU for the less-responsive mouse subpopulation (rate: 0.0129 $\log_{10}$ CFU/week), while treatment with 25 mg/kg BDQ as well as BDQ plus PZA showed similar decreases in pulmonary CFU (rate approximately 0.28 $\log_{10}$ CFU/week) for the less-responsive subpopulation. Calculations for the responsive mouse populations suggested similar decreases in bacterial load for BDQ alone as well as the BDQ-PZA groups (rates between 0.21 and 0.43 $\log_{10}$ CFU/week).

To determine the contribution of drug-resistant mutants to the differential treatment response, lung homogenates were simultaneously plated on agar plates with and without BDQ. BDQ resistant mutants comprised less than 1% of total bacterial CFU in the lung following 4 weeks of treatment (data not shown), with 4 out of 6 mice having detectable numbers of resistant colonies on agar containing 0.5 μg/mL BDQ, demonstrating that the divergent treatment response was not the result of bacterial drug resistance.

BDQ/PZA Combination Therapy Was Effective in BALB/c Mice and against Both Subpopulations of C3HeB/FeJ Mice. Mice were treated with 10 mg/kg BDQ and 150 mg/kg PZA to determine efficacy of the combination regimen in both BALB/c and C3HeB/FeJ mice. In BALB/c mice, combination therapy was highly effective as expected, resulting in a 4.1 $\log_{10}$ CFU reduction after 4 weeks of treatment ($P < 0.005$), with a highly uniform treatment response throughout (Figure 3A). This result was similar to

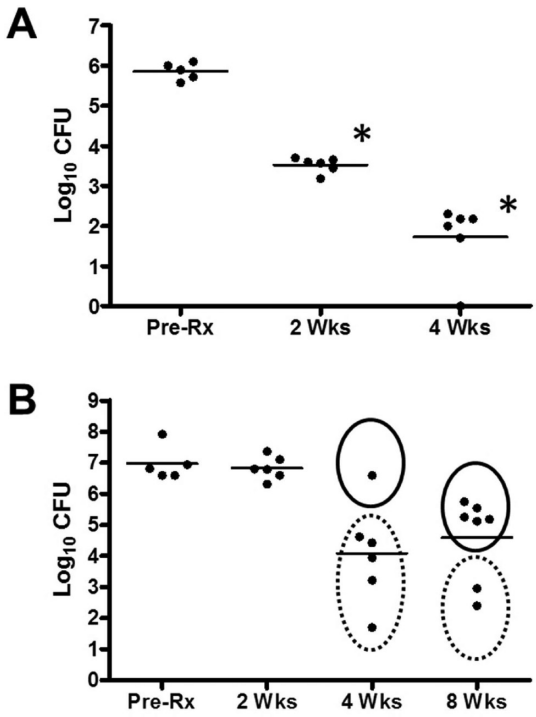

Figure 3. BDQ/PZA combination therapy had activity against both subpopulations in C3HeB/FeJ mice. Plots represent $\log_{10}$ CFU determinations from the lungs of individual BALB/c (A) or C3HeB/FeJ (B) mice. Pre-Rx represents untreated mice 8 weeks following aerosol infection. Mice were treated with BDQ 10 mg/kg and PZA 150 mg/kg in combination via oral gavage. BALB/c mice were treated for either 2 or 4 weeks. C3HeB/FeJ mice were treated for either 2, 4, or 8 weeks. Ovals with solid lines represent the less-responsive subpopulation, and dashed lines represent the responsive subpopulation of C3HeB/FeJ mice. Pre-Rx and defined time points were determined to be statistically different (*; $P < 0.01$) using a one-way ANOVA. Responsive and less-responsive populations were determined to be statistically different ($P < 0.001$) using a two-way ANOVA.

previously published results in Swiss mice.[26] In C3HeB/FeJ mice, a heterogeneous treatment response was again visible after BDQ + PZA treatment resulting in two different mouse populations whereby significantly more drug activity was observed in one subgroup when compared to the other ($P < 0.001$). In the less-responsive subpopulation (Figure 3B; solid circles), a substantial 1.6 $\log_{10}$ CFU reduction was observed following 8 weeks of treatment. In the responsive subpopulation (Figure 3B; dashed circles), a 3.4 $\log_{10}$ CFU reduction was observed by 4 weeks of treatment, which increased to a 4.3 $\log_{10}$ reduction after 8 weeks. Taken into account that the

DOI: 10.1021/acsinfecdis.5b00127
ACS Infect. Dis. 2016, 2, 251−267

division in responsive and less-responsive mouse population is somewhat arbitrary, the addition of PZA to a low BDQ dosage suggests under these experimental conditions a significant benefit in reducing the bacterial load in lungs primarily against the BDQ less-responsive subpopulation (observed in Figure 2C; solid circles; $P < 0.001$).

In the spleens of C3HeB/FeJ mice where caseous necrotic pathology is absent, a highly uniform treatment response was observed following treatment with PZA, BDQ, and BDQ plus PZA (Supplemental Figure 1). Treatment efficacy and experimental variation were similar between BALB/c and C3HeB/FeJ mice.

Pharmacokinetic Noncompartmental Analysis. We next wanted to examine whether mouse strain specific pharmacokinetic (PK) differences could account for the divergent treatment response observed in BALB/c and C3HeB/FeJ mice. For the PK analysis, mice were administered a single oral dose of PZA (150 mg/kg) or BDQ (25 mg/kg). Plasma, whole lung (cranial, medial, and accessory lung lobes), dissected regions of uninvolved lung, and dissected lesions from BALB/c and C3HeB/FeJ mice were collected for LC/MS/MS quantification of drug levels. In BALB/c mice, cellular non-necrotizing lesions (type III lesions) were collected, while in C3HeB/FeJ mice, only encapsulated caseous necrotic granulomas (type I) were collected. Mean drug concentration values for each time point and each tissue type were used to construct plasma and tissue concentration−time profiles for PZA and its primary metabolite POA (Figure 4), and BDQ and the M2 metabolite (Figure 5) in parallel groups of *M. tuberculosis* infected BALB/c and C3HeB/FeJ mice.

These profiles revealed very rapid absorption of PZA and rapid elimination, which was similar between BALB/c and C3HeB/FeJ mice, as described before.[27,28] Plasma concentrations for PZA and POA were similar between both mouse strains. In addition, no lesion-specific differences in absorption were observed as the concentration−time profile of PZA and POA for type III lesions in BALB/c mice was very similar to that of the type I caseous necrotic granulomas in C3HeB/FeJ mice. BDQ also exhibited very rapid absorption, coupled with extremely slow elimination which was similar between both mouse strains and as described before.[26] Although plasma concentrations were similar between BALB/c and C3HeB/FeJ mice, both BDQ and M2 were found in far lower concentrations in the type I caseous necrotic granulomas as compared to the type III cellular lesions (Figure 5).

Noncompartmental analysis was performed on the mean values to calculate C_{max}, t_{max}, $t_{1/2}$, and AUC through the 8 h interval for PZA and its metabolite (Table 2), or the 168 h interval for BDQ and its metabolite (Table 3). Similar plasma exposures as measured by AUC analysis were observed in both BALB/c and C3HeB/FeJ mice for PZA, BDQ, and M2. This demonstrated that mouse strain specific differences in plasma PK were not responsible for the differential drug activity observed in the described efficacy experiments. However, the plasma exposure of C3HeB/FeJ mice to POA was approximately half that seen in BALB/c mice. The reason for this is unclear at this time.

Within lung tissue, PZA and POA drug levels were similar between BALB/c and C3HeB/FeJ mice when comparing whole lung, dissected uninvolved lung, and dissected lesions. AUC_{tissue} to AUC_{plasma} ratios were calculated to estimate how readily drug partitioned from plasma into the lung. PZA and POA partitioned into lung tissue, cellular lesions, and caseous

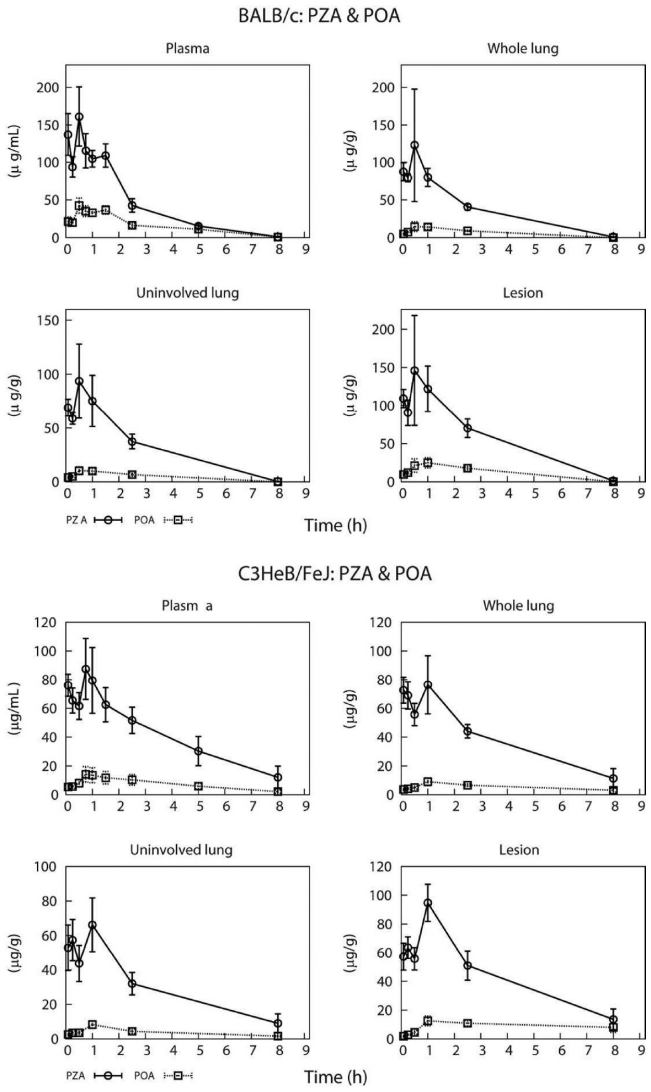

Figure 4. Plasma and lung tissue concentration−time profiles of PZA and POA in BALB/c and C3HeB/FeJ mice following a single 150 mg/kg PZA oral dose. Data points indicate mean values (n = 5 mice per time point) with SD error bars.

necrotic granulomas with similar efficiency indicating that caseous necrotic granulomas did not impede drug penetration.

High AUC_{tissue} to AUC_{plasma} ratios for BDQ and especially for M2 were observed (Table 3), consistent with the known long half-life and high protein binding biochemical characteristics of BDQ.[26] Similar drug exposures were seen for BDQ and M2 between BALB/c and C3HeB/FeJ mice by analysis of whole lung and dissected uninvolved lung samples. It was only by comparison of dissected lesions that significant differences in drug accumulation were observed that were dependent upon the lesion type studied. Approximately 2.5 times less BDQ and M2 were found within the caseous necrotic granulomas of C3HeB/FeJ mice when compared to the cellular lesions in BALB/c mice, reflected by the AUC_{168} exposure for BDQ of 949 μg·h/g in BALB/c cellular lesions versus 387.1 μg·h/g in caseous necrotic granulomas of C3HeB/FeJ mice; and an AUC_{168} for M2 of 7619 μg·h/g in BALB/c lesions versus 2848 μg·h/g in C3HeB/FeJ granulomas. Therefore, lesion-specific characteristics between mouse strains (i.e., the concentration of macrophages) had a significant impact upon the accumulation

DOI: 10.1021/acsinfecdis.5b00127
ACS Infect. Dis. 2016, 2, 251−267

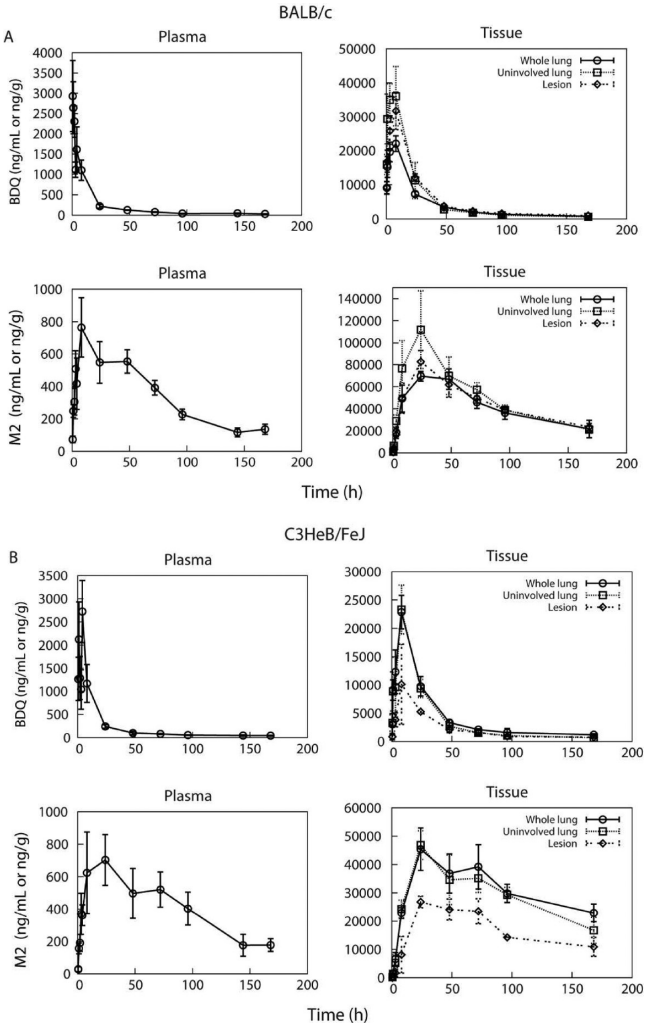

Figure 5. Plasma and lung tissue concentration−time profiles of BDQ and M2 in BALB/c and C3HeB/FeJ mice following a single 25 mg/kg BDQ oral dose. Data points indicate mean values (n = 5 mice per time point) with SD error bars.

of BDQ and M2, which was not observable when examining whole lung samples.

After BDQ treatment, 7−10 times more M2 was present in the lung tissue and dissected lesions of BALB/c and C3HeB/FeJ mice when compared to BDQ (Table 3). Knowing that the MIC of M2 is approximately five times higher than that of BDQ suggests that M2 contributes a significant proportion of the total efficacy observed in mice, as has been described before.[26]

Pharmacokinetic Compartmental Analysis. To provide better estimates of parameter variability, a compartmental analysis was performed for PZA, POA, BDQ, and M2. A one-compartment model was utilized for PZA and POA (Supplemental Figure 2) using first order absorption and elimination as previously reported,[29] and was used to estimate PK parameters summarized in Supplemental Table 1. Plots illustrating goodness of model fit to mean data and 95% confidence intervals are shown in Supplemental Figure 3. A three-compartment model was used for BDQ and M2[30] to estimate PK parameters shown in Supplemental Table 2, and plots illustrating goodness of model fit to mean data and 95% confidence intervals are shown in Supplemental Figure 4. A comparison of absorption (k_a), clearance (CL), and volume of distribution (V) parameters failed to identify significant differences between BALB/c and C3HeB/FeJ mice for PZA and POA with the exception that the clearance of POA in C3HeB/FeJ mice was slower than in BALB/c mice (Figure 6A). Similar plasma PK parameters were also observed for both mouse strains for BDQ and M2 (Figure 7A). Analysis of the penetration coefficient (PC) data showed that PZA accumulated to a similar degree in BALB/c and C3HeB/FeJ lesions, while POA accumulated within C3HeB/FeJ granulomas to a greater degree than the cellular BALB/c lesions (Figure 6B). The largest differences were seen with BDQ, which had a PC of 31.07 in BALB/c mice and 15.68 in C3HeB/FeJ mice, and with M2 (Figure 7B) which showed a similar trend in PC values of 144.70 and 63.41 in BALB/c and C3HeB/FeJ mice, respectively (Supplemental Table 2).

Table 2. Noncompartmental Analysis of Mean Plasma and Lung Tissue Concentrations of PZA and POA in BALB/c and C3HeB/FeJ Mice Following a Single 150 mg/kg Oral Dose of PZA[a]

		BALB/c		C3HeB/FeJ	
sample	param (units)	PZA	POA	PZA	POA
plasma	C_{max} (μg/mL)	161.2	42.5	87.4	14.2
	t_{max} (h)	0.5	0.5	0.75	0.75
	AUC_{8h} (μg·h/mL)	346.1	127.3	328.9	58.7
	$t_{1/2}$ (h)	1.05	1.24	2.6	2.4
whole lung	C_{max} (μg/g)	122.7	14.7	76.5	9.00
	t_{max} (h)	0.5	0.5	1.0	1.0
	AUC_{8h} (μg·h/g)	298.6	53.7	306.3	43.9
	$t_{1/2}$ (h)	1.02	0.24	2.82	5.13
	AUC_{WL}/AUC_{plasma}	0.86	0.42	0.93	0.75
uninvolved lung	C_{max} (μg/g)	93.6	10.3	66.2	8.3
	t_{max} (h)	0.5	0.5	1.0	1.0
	AUC_{8h} (μg·h/g)	262.8	39.0	237.9	30.4
	$t_{1/2}$ (h)	0.75	0.24	3.01	3.90
	AUC_{UL}/AUC_{plasma}	0.76	0.31	0.72	0.52
lesion	C_{max} (μg/g)	146.2	25.0	94.7	12.5
	t_{max} (h)	0.5	1.0	1.0	1.0
	AUC_{8h} (μg·h/g)	459.4	99.5	351.8	75.1
	$t_{1/2}$ (h)	0.96	0.83	2.88	12.1
	AUC_{Les}/AUC_{plasma}	1.33	0.78	1.07	1.28

[a] AUC_{8h} was calculated using the linear trapezoidal rule. $t_{1/2}$ was calculated from a terminal elimination rate obtained by linear regression on the log-transformed 2.5−8 h concentration measurements.

Together, the concentration−time profile analysis, noncompartmental analysis, and compartmental modeling of the PK data revealed that BDQ, PZA, and their major metabolites behaved similarly in BALB/c and C3HeB/FeJ mice in both plasma and whole lung tissue samples. The only substantial difference that emerged from these experiments was the lesion-specific decreased accumulation of BDQ and M2 within caseous necrotic granulomas of C3HeB/FeJ mice compared to the cellular lesions of BALB/c mice.

MALDI-MSI Revealed Lesion-Specific Differences in the Distribution of BDQ and M2. The AUC exposure estimates and PC determinations described above showed quantitatively that drug levels for BDQ and M2 were reduced by approximately half in mature necrotic type I granulomas of C3HeB/FeJ mice compared to BALB/c lesions. To examine drug distribution within the lung and within pulmonary lesions, a newer imaging modality was used that allows the visualization

DOI: 10.1021/acsinfecdis.5b00127
ACS Infect. Dis. 2016, 2, 251−267

Table 3. Noncompartmental Analysis of Mean Plasma and Lung Tissue Concentrations of BDQ and M2 in BALB/c and C3HeB/FeJ Mice Following a Single 25 mg/kg Oral Dose of BDQ[a]

		BALB/c		C3HeB/FeJ	
sample	param (units)	BDQ	M2	BDQ	M2
plasma	C_{max} (μg/mL)	2.93	0.76	2.72	0.70
	t_{max} (h)	0.5	8	4	24
	AUC_{168h} (μg·h/mL)	33.7	57.3	35.9	69.3
	$t_{1/2}$ (h)	89.3	59.8	116.4	55.9
whole lung	C_{max} (μg/g)	22.1	69.5	22.9	45.4
	t_{max} (h)	8	24	8	24
	AUC_{168h} (μg·h/g)	694.0	7207	739.42	5254
	$t_{1/2}$ (h)	74.5	90.6	130.0	134.7
	AUC_{WL}/AUC_{plasma}	20.6	125.7	20.6	75.8
uninvolved lung	C_{max} (μg/g)	36.0	111.8	23.3	46.9
	t_{max} (h)	8	24	8	24
	AUC_{168h} (μg·h/g)	956.6	8825	653.9	4895
	$t_{1/2}$ (h)	67.4	69.7	84.1	89.4
	AUC_{UL}/AUC_{plasma}	28.4	153.9	18.2	70.7
lesion	C_{max} (μg/g)	31.7	82.7	10.1	26.8
	t_{max} (h)	8	24	8	24
	AUC_{168h} (μg·h/g)	949.6	7619	387.1	2848
	$t_{1/2}$ (h)	85.5	90.7	104.4	98.6
	AUC_{Les}/AUC_{plasma}	28.2	132.9	10.8	41.1

[a]AUC_{168h} was calculated using the linear trapezoidal rule. $t_{1/2}$ was calculated from a terminal elimination rate obtained by linear regression on the log-transformed 72−168 h concentration measurements.

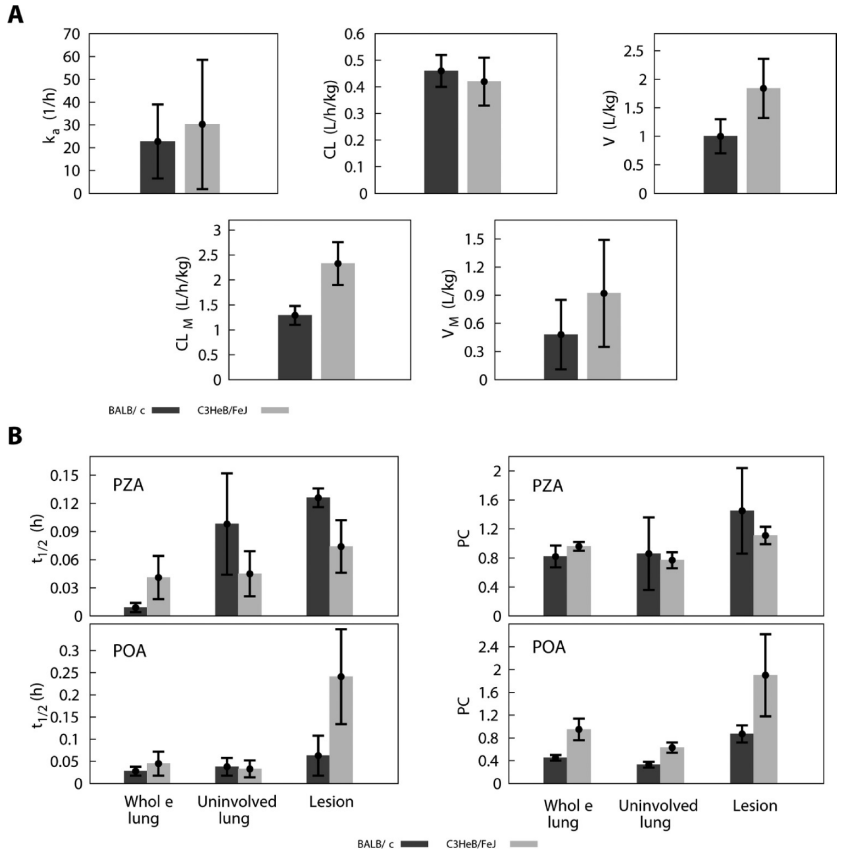

Figure 6. Arithmetic mean and SD for BALB/c and C3HeB/FeJ plasma and lung tissue population PK parameters for PZA and POA. Panel A shows a comparison of absorption (k_a), clearance (CL), and volume of distribution (V) parameters for PZA and POA in both mouse strains. Panel B shows a comparison of half-life ($t_{1/2}$) and penetration (PC) coefficient for PZA and POA in both mouse strains. Histogram height represents the arithmetic mean, with error bars representing mean ± SD. The tissue equilibrium half-life was calculated as $t_{1/2} = \ln(2)/k$, where k is the corresponding tissue penetration rate. All values were calculated from the corresponding GM and GSD listed in Supplemental Table 1.

DOI: 10.1021/acsinfecdis.5b00127
ACS Infect. Dis. 2016, 2, 251−267

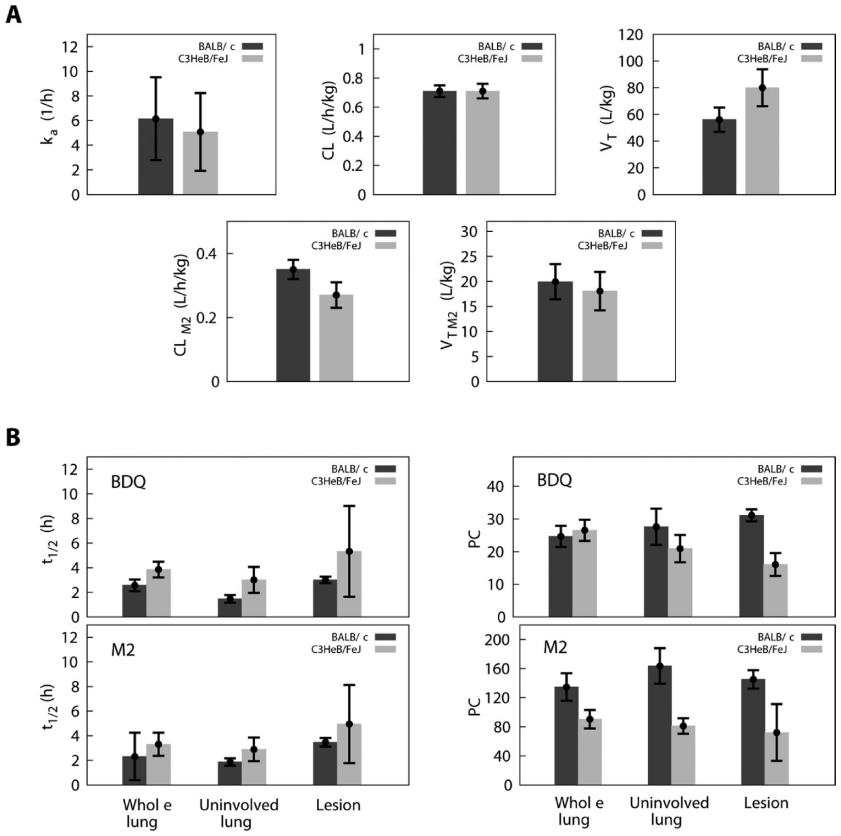

Figure 7. Arithmetic mean and SD for BALB/c and C3HeB/FeJ plasma and lung tissue population PK parameters for BDQ and M2. Panel A shows a comparison of absorption (k_a), clearance (CL), and volume of distribution (V) parameters for BDQ and M2 in both mouse strains. Panel B shows a comparison of half-life ($t_{1/2}$) and penetration (PC) coefficient for BDQ and M2 in both mouse strains. Histogram height represents the arithmetic mean, with error bars representing mean ± SD. The tissue equilibrium half-life was calculated as $t_{1/2} = \ln(2)/k$ where k is the corresponding tissue penetration rate. All values were calculated from the corresponding GM and GSD listed in Supplemental Table 2.

of unlabeled drugs in tissue sections. MSI is a semiquantitative approach, and the results therefore only show a qualitative visual representation of relative drug distribution.[31] BALB/c and C3HeB/FeJ mice were administered a single dose of PZA (150 mg/kg), and samples were collected and prepared for MALDI-MSI analysis. Visual examination of the drug distribution map for PZA and for POA (Figures 8 and 9) indicated that t_{max} occurred between 0.5 and 1 h postdose. It was also visually apparent that PZA was present in greater amounts when compared to POA. The t_{max} visualized by the MALDI-MSI analysis displayed a high degree of concordance with the t_{max} values determined by noncompartmental analysis which was performed on the mean whole lung tissue concentrations (shown in Table 2).

MALDI-MSI was also performed on lungs obtained from BALB/c and C3HeB/FeJ mice treated with a single dose of 25 mg/kg BDQ (Figures 10 and 11). Although not as clearly apparent as with PZA, the t_{max} for BDQ occurred at 3 h postdose, while the t_{max} for the primary M2 metabolite occurred at 24 h. As with PZA and POA, these t_{max} results were similar to the values obtained from the noncompartmental analysis (Table 3).

MSI was next utilized to identify patterns of lesion-specific drug distribution. Caseous necrotic granulomas were identified based upon histological examination of hematoxylin and eosin stained serial sections. MALDI-MSI analysis revealed that PZA and POA readily distributed into the cellular lesions of BALB/c mice (Figure 8, circles) as well as the caseum of type I granulomas in C3HeB/FeJ mice (Figure 9, circles), and exhibited relatively homogeneous distribution of drug throughout the lung.

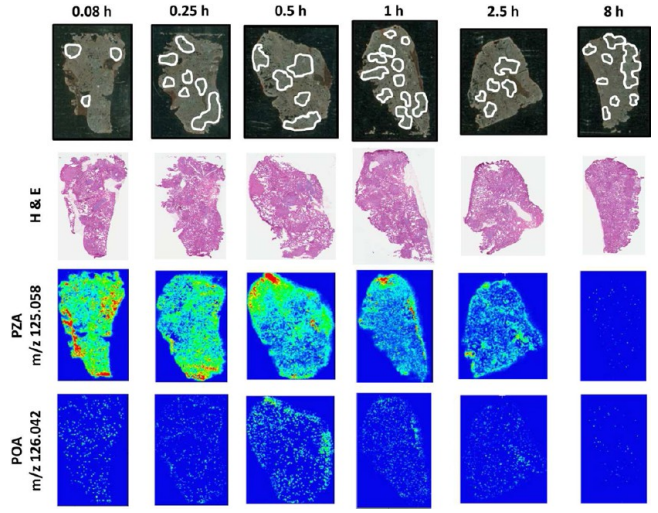

Figure 8. MALDI-MS time course images of PZA and POA in BALB/c mice acquired 0.08−8 h following a single oral 150 mg/kg dose of PZA. Cellular, non-necrotizing lesions (type III) are outlined in white. Images depict a single lung lobe obtained from a representative mouse (n = 4 mice per time point). A serial section was stained with hematoxylin and eosin (H&E) for comparison.

DOI: 10.1021/acsinfecdis.5b00127
ACS Infect. Dis. 2016, 2, 251−267

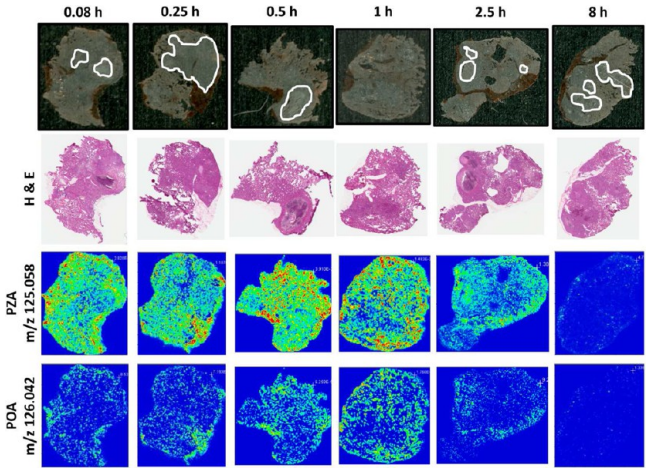

Figure 9. MALDI-MS time course images of PZA and POA in C3HeB/FeJ mice acquired 0.08−8 h following a single oral 150 mg/kg dose of PZA. Caseous necrotic granulomas (type I) are outlined in white. Images depict a single lung lobe obtained from a representative mouse (n = 4 mice per time point). A serial section was stained with hematoxylin and eosin (H&E) for comparison.

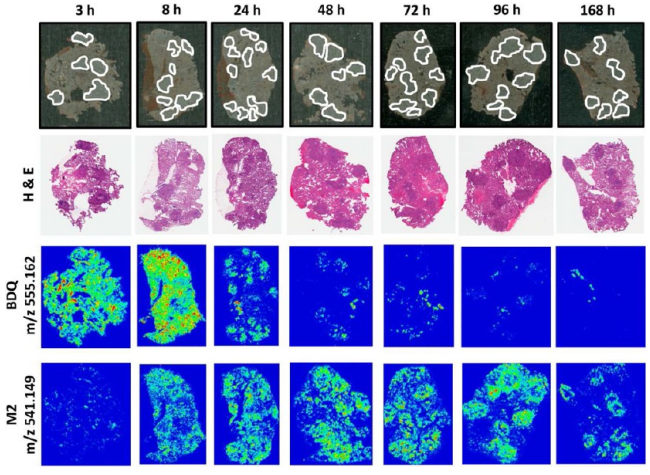

Figure 10. MALDI-MS time course images of BDQ and M2 in BALB/c mice acquired 8−168 h following a single oral 25 mg/kg dose of BDQ. Cellular, non-necrotizing lesions (type III) are outlined in white. Images depict a single lung lobe obtained from a representative mouse (n = 4 mice per time point). A serial section was stained with hematoxylin and eosin (H&E) for comparison.

BDQ and M2 were observed to accumulate within histologically normal lung tissue of both BALB/c and C3HeB/FeJ mice. High levels of BDQ and M2 accumulated within the cellular lesions of BALB/c mice. In C3HeB/FeJ mice, mature type I granulomas consist of a central caseous necrotic region primarily composed of large numbers of neutrophils and macrophages. The caseum is surrounded by a rim of foamy macrophages containing large numbers of intracellular bacteria, which are retained within a collagen capsule. Peripheral to the capsule is a highly cellular zone of macrophages, epithelioid macrophages, and lymphocyte clusters.[6] It was observed that BDQ and M2 were present at high levels in the cellular regions surrounding the caseum of mature type I granulomas with low levels of both compounds being detected within the caseum. Analysis of MALDI-MS images that were acquired by purposefully saturating the signal intensity scale failed to detect BDQ or M2 within the central

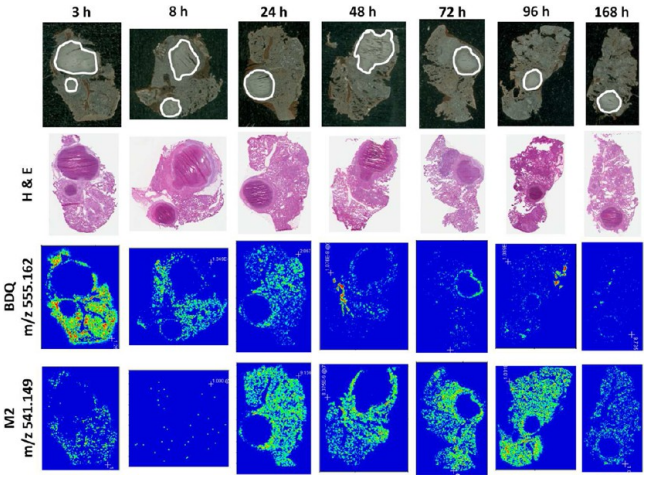

Figure 11. MALDI-MS time course images of BDQ and M2 in C3HeB/FeJ mice acquired 8−168 h following a single oral 25 mg/kg dose of BDQ. Caseous necrotic granulomas (type I) are outlined in white. Images depict a single lung lobe obtained from a representative mouse (n = 4 mice per time point). A serial section was stained with hematoxylin and eosin (H&E) for comparison.

caseum of the granuloma (Figure 12). To estimate the limit of detection of the MALDI-MSI methodology for BDQ, serial

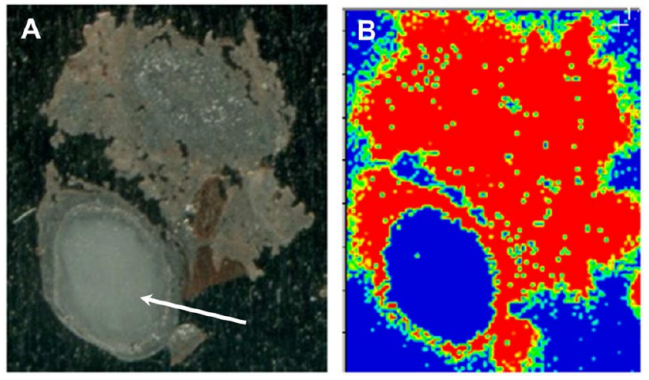

Figure 12. Reduced penetration of BDQ into caseous necrotic granulomas. Light micrograph of a caseous necrotic granuloma (A; arrow) and a corresponding MALDI-MS image (B) acquired with a saturated intensity scale showing no detectable BDQ within the central caseum of the granuloma. Representative MALDI-MS image of a single lung lobe obtained from a C3HeB/FeJ mouse (n = 5). Mice were given a single 25 mg/kg oral dose of BDQ 1 h prior to necropsy.

dilutions of BDQ were spotted onto human or mouse lung tissue containing mature caseous necrotic granulomas. MSI analysis determined that the limit of detection was approximately 1.2 μg/g, which is more than 20 times the MIC for this compound. Care should therefore be exercised when examining the BDQ and M2 images, as biologically relevant concentrations of drug undetectable by MALDI-MSI were most likely present within caseum in mice following a single dose of 25 mg/kg.

Closer analysis of the characteristics of BDQ and M2 accumulation in caseous necrotic granulomas showed pronounced accumulation of drug within the cellular layers containing activated macrophages and lymphocytes external to the collagen capsule. It was also observed that BDQ appeared to penetrate more deeply into these granulomas than

DOI: 10.1021/acsinfecdis.5b00127
ACS Infect. Dis. 2016, 2, 251−267

M2, and accumulated within the histologically distinct rim of foamy macrophages known to contain large numbers of intracellular bacilli (Figure 13). BDQ also appeared to persist within the foamy macrophage rim for a longer duration in comparison to other regions of the lung (Figure 13 and Figure 11, BDQ 72 and 96 h).

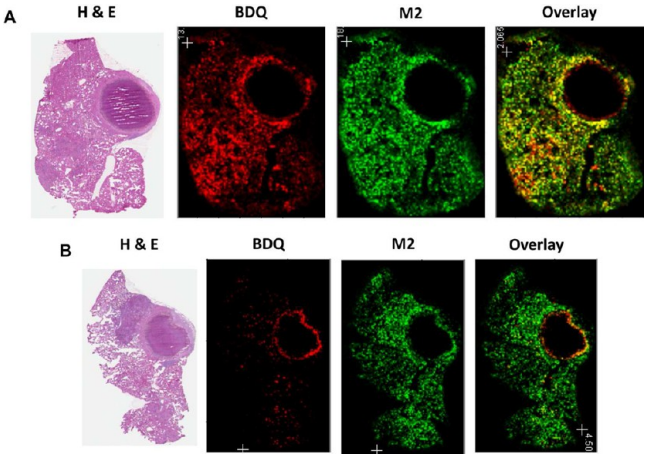

Figure 13. Differential penetration of BDQ and M2 (*N*-desmethyl-BDQ) into caseous necrotic granulomas. MALDI-MS images of BDQ (red) and M2 (green) acquired 24 h (A) and 72 h (B) following a single oral 25 mg/kg dose of BDQ. Images represent a single lung lobe obtained from C3HeB/FeJ mice.

BDQ Accumulated to a High Degree within THP-1 Cells. To confirm the observation that BDQ accumulated within the rim of foamy macrophages, we performed an in vitro assay using the THP-1 monocyte cell line. To determine the intracellular-to-extracellular ratio of PZA, POA, and BDQ, cells were exposed to drug for 30 min and rinsed extensively. Lysates were prepared and analyzed by LC/MS/MS. PZA and POA accumulated to a very low degree within THP-1 cells (Figure 14). BDQ, however, was readily taken up by THP-1 cells as evidenced by an intracellular-to-extracellular ratio more than 30 times greater than for PZA.

The diverse spectrum of morphologically distinct pulmonary lesion types found within TB patients encompasses a variety of

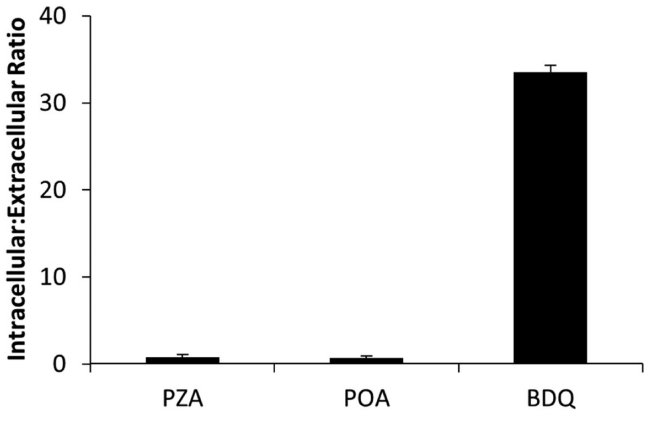

Figure 14. BDQ accumulated to a greater degree within THP-1 cells. THP-1 cells were exposed to 1 mM PZA, 0.4 mM POA, or 0.5 mM BDQ. Intracellular-to-extracellular ratios were calculated based upon LC/MS/MS quantification of drug levels following washing and cell lysis.

microenvironmental conditions which are challenging to replicate in mouse models that fail to exhibit hypoxic, caseous necrotic granulomas. Microenvironmental conditions can have pronounced effects upon treatment efficacy due to drug penetration, drug accumulation, hypoxic conditions, pH, and/or altered nutrient sources. In turn, these environmental conditions can affect the replicative and metabolic state of the bacteria located therein. In a previous publication, our group identified that the caseous necrotic pathology exhibited by C3HeB/FeJ mice following LDA infection with *M. tuberculosis* Erdman resulted in decreased treatment response to CFZ.[6] Treatment prior to the formation of caseous necrotic granulomas displayed similar efficacy when compared to BALB/c mice. The decreased treatment response appeared to be linked to the hypoxic nature of advanced, caseous necrotic granulomas. A recent manuscript also identified a divergent treatment response to PZA, which was related to the intragranuloma pH.[9]

In the present study, we observed that treatment with a low dose of BDQ resulted in two distinct treatment responses in C3HeB/FeJ mice, whereby one mouse subpopulation responded effectively to the drug and another was far less responsive. In BALB/c mice which do not develop caseous necrotic granulomas, treatment response was highly uniform with only one mouse population evident which responded effectively to treatment. Treatment with the standard 25 mg/kg dose of BDQ increased both the magnitude of the treatment response and the number of mice in the responding group. Furthermore, the addition of PZA to low dose BDQ showed that this combination had efficacy against both the BDQ responsive and BDQ less-responsive subpopulations in C3HeB/FeJ mice. A comprehensive PK analysis of drug exposure in plasma and tissue levels in lungs ruled out differences between mouse strains as being the predominant cause of the differential treatment response. Although C3HeB/FeJ mice have more than 2 orders of magnitude more bacteria within the lung compared to BALB/c mice and have concomitantly more BDQ resistant mutants, this alone could not explain the emergence of two mouse subpopulations as BDQ resistant mutants comprised only a small minority (<1%) of total bacterial CFU in the lungs following 4 weeks of treatment.

Characterization of the PK properties for most TB drugs is typically performed by assessment of drug levels in plasma and lungs of uninfected mice. However, it is important to appreciate that serum drug exposure may not correlate with exposure at the site of infection,[28,32] and that histologically distinct lesion types may differentially impact drug partitioning.[33] In this study, we specifically quantified drug levels in plasma, whole lung lobes, dissected regions of uninvolved lung, cellular non-necrotizing lesions from BALB/c mice, and caseous necrotic granulomas and dissected caseum from C3HeB/FeJ mice by quantitative LC/MS/MS analysis. PZA and POA were shown to distribute to lung tissue from the plasma and to readily penetrate both cellular lesions and caseous necrotic granulomas to a similar extent. PZA exposure in the plasma of BALB/c mice was 346.1 μg·h/mL, with similar exposures of 262.8 μg·h/g seen in uninvolved lung tissue and slightly higher levels of 459.4 μg·h/g observed in dissected lesions. These results were similar to those observed in C3HeB/FeJ mice. In BALB/c mice, POA exposures were 127.3 μg·h/mL in the plasma, 39.0 μg·h/g in uninvolved lung, and 99.5 μg·h/g in lesions. For the metabolite, C3HeB/FeJ mice had a plasma exposure of 58.7 μg·

DOI: 10.1021/acsinfecdis.5b00127
ACS Infect. Dis. 2016, 2, 251−267

h/mL, which was approximately half that of BALB/c mice. A similar trend was observed in the uninvolved lung tissue of C3HeB/FeJ mice where a lower POA exposure of 30.4 μg·h/g was seen, with higher exposure (75.1 μg·h/g) found within caseous granulomas. In summary though, PZA levels in plasma, lungs, and lesions were found to be very similar between BALB/c and C3HeB/FeJ mice.

For BDQ, similarly low plasma levels were observed in BALB/c and C3HeB/FeJ mice of 33.7 μg·h/mL and 35.9 μg·h/mL, respectively. Significantly higher levels of BDQ were observed in the tissues, with 956.6 μg·h/g in BALB/c mice and 653.9 μg·h/g in C3HeB/FeJ mice. Within the cellular lesions of BALB/c mice, higher drug exposure levels of 949.6 μg·h/g were seen, reflecting the accumulation of drug within immune cells. Substantially lower levels of BDQ (387.1 μg·h/g) were present in the caseous necrotic granulomas of C3HeB/FeJ mice when compared to the BALB/c cellular lesions. When the highly cellular layers of the type I granulomas were removed and isolated caseum was analyzed by LC/MS/MS, even lower levels of BDQ (974.5 ng/g) were present at 8 h following a single 25 mg/kg dose.

The M2 metabolite was also present at similar levels in BALB/c and C3HeB/FeJ mice in the plasma (57.3 μg·h/mL and 69.3 μg·h/g, respectively). M2 tissue levels were substantially higher, as reflected by the drug exposure of 8825 μg·h/g in BALB/c mice and 4895 μg·h/g in C3HeB/FeJ mice. Dissected BALB/c lesions had 7619 μg·h/g of M2, with substantially lower levels of 2848 μg·h/g found in C3HeB/FeJ granulomas. Again, a preliminary analysis of dissected caseum revealed that M2 was present at substantially lower concentrations (587.5 ng/g) than that seen in intact dissected lesions.

With the exception of POA, similar PK properties were observed between BALB/c and C3HeB/FeJ mice in plasma for PZA, BDQ, and M2, suggesting that the differences in treatment response were not due to mouse strain differences in drug absorption or elimination. It is not known why C3HeB/FeJ mice had approximately half the POA exposure compared to BALB/c mice when exposure to the parent compound was similar between mouse strains (Table 2). Recent work by Via et al. demonstrated that host-mediated conversion of PZA to POA accounted for the majority of circulating POA in preclinical animal models.[28] A slower conversion from PZA to POA, a larger volume of distribution for POA, or more rapid elimination of POA by C3HeB/FeJ mice as seen in Figure 6B could explain these results.

Both BDQ and M2 were able to partition to cellular lesions of BALB/c mice with similar efficiency when compared to uninvolved lung tissue. However, in C3HeB/FeJ mice with caseous necrotic granulomas, less than half the amount of BDQ and M2 was found within caseous necrotic granulomas as compared to cellular lesions in BALB/c mice. Importantly, the lower levels of BDQ and M2 in caseous granulomas were not evident from the homogenized whole lung samples, only becoming apparent when granulomas were dissected and analyzed. Lesion-specific PK analysis may therefore represent an important consideration for the development of novel TB drugs.

The primary advantage of the MALDI-MSI technique is that high resolution mapping of relative drug concentrations within the lung can be obtained and combined with lesion-specific pathological analysis. This information could not have been obtained from conventional LC/MS/MS analysis, as the precise spatial distribution of drug within a tissue is lost during the homogenization and preparation process. Subsequent MALDI-MSI analysis corroborated the PK findings, and provided additional insights into the lesion-specific partitioning characteristics of the drugs examined in this study. Distribution of PZA and POA was observed to be relatively homogeneous within the lung and throughout the lesions of BALB/c and C3HeB/FeJ mice. The levels of BDQ and its primary metabolite within caseous necrotic granulomas of C3HeB/FeJ mice were significantly lower when compared to the levels found within cellular non-necrotizing lesions in BALB/c mice and uninvolved lung tissue. Furthermore, MALDI-MSI analysis allowed us to determine that high levels of BDQ and M2 accumulated within the cellular regions of caseous necrotic granulomas that lie outside of the collagen capsule, while relatively little BDQ and M2 partitioned into the caseum. This was similar to earlier results described for moxifloxacin using a rabbit model of TB infection.[33]

Although the MALDI-MSI images failed to show any detectable BDQ or M2 within the caseum, care must be taken in the interpretation of these results. Recognition that high levels of drug accumulated along the exterior margins of granulomas immediately adjacent to the caseum suggested that our LC/MS/MS quantification of BDQ and M2 in dissected granulomas may have overrepresented the amount of drug specifically found within the central caseum. Subsequently, a preliminary LC/MS/MS quantitation of BDQ and M2 from carefully dissected caseum of type I granulomas in C3HeB/FeJ mice treated with a single 25 mg/kg dose of BDQ contained 974.5 ng/g of BDQ and 587.5 ng/g of M2 at 8 h post treatment, which was significantly less than that obtained from grossly dissected type I granulomas (Figure 5). These results were similar to those observed in plasma, and still greater than the MIC for both compounds. Therefore, it would be erroneous to assume that no BDQ or M2 penetrated into the caseum based entirely on the MALDI-MS images. MALDI-MSI is a semiquantitative analytical tool[31] with a limit of detection for BDQ in caseum estimated to be 1.2 μg/g. This concentration is more than 20 times the MIC (determined in the presence of protein) for BDQ, showing that MALDI-MSI is relatively insensitive for BDQ in lung tissue. BDQ is a highly potent drug, and amounts undetectable by MALDI-MSI could still be sufficient to have a pronounced effect on bacteria within the caseum. Considering that BDQ and M2 are more than 99% protein bound,[26] the combination of low drug levels found in caseum and the high protein binding of the drug may explain the reduced efficacy seen in C3HeB/FeJ studies described here, especially in the case where the lower dosage of BDQ was evaluated. We also showed that the reduced efficacy in a subpopulation of C3HeB/FeJ mice with the lower dosage of BDQ could be overcome either by a higher dose of BDQ or by combining BDQ with PZA. These results underscore the importance of treating patients with a sufficient BDQ dosage and of careful consideration of companion drugs when designing clinical treatment regimens.

Using MSI, we were further able to identify that BDQ accumulated within the rim of foamy macrophages which contained large numbers of intracellular bacilli[6] and persisted within these cells longer than in other areas of the lung. The tendency of BDQ to accumulate to a high degree within macrophages[34] was confirmed by the high intracellular-to-extracellular ratio observed in the in vitro drug accumulation assay. Preferential accumulation within macrophages, high

DOI: 10.1021/acsinfecdis.5b00127
ACS Infect. Dis. 2016, 2, 251−267

tissue-to-plasma distribution, and long terminal half-life are also observed with CFZ, another cationic amphiphilic TB drug which has similar biochemical properties.[35,36] Recently, it was shown using MALDI-MSI and LC/MS/MS quantification that CFZ failed to efficiently penetrate caseous granulomas obtained from TB patients with results that were similar to those observed in C3HeB/FeJ mice for BDQ in this study.[37] It is important to appreciate that while cationic amphiphilic drugs may accumulate to very high levels within macrophages, the drug may be sequestered in lysosomal compartments and therefore not be accessible to the bacteria. While M2 did not accumulate within the rim of foamy macrophages to the same extent as BDQ as shown by MALDI-MSI, M2 did accumulate within lungs and lesions of BALB/c and C3HeB/FeJ mice at 7−10 times greater levels when compared to the parent compound. Since the in vivo activity of M2 is approximately one-fifth that of BDQ, this suggests that M2 was contributing equally with the parent compound BDQ to the observed in vivo efficacy in mice. Since conversion of BDQ to M2 is significantly lower in humans,[26] greater efficacy within mature granulomas may be achievable than that observed in this mouse model.

Treatment with PZA resulted in two distinct treatment responses in C3HeB/FeJ mice, albeit to a lesser extent than observed for BDQ, whereby one mouse subpopulation responded effectively to the drug and another was far less responsive. The treatment results for PZA were, however, not dose-dependent, which suggested that the efficacy of PZA may depend upon environmental factors within the lesion or the metabolic state of the bacilli. The highly uniform distribution of PZA and its metabolite POA observed in the PK analysis (Table 2) and the MALDI-MS images (Figure 9) confirmed that PZA distributed across granuloma caseum similarly to that observed in rabbits and in humans.[28] However, it is known that the MIC of PZA increases with increasing pH when evaluated under standard laboratory culture conditions[38] (MIC > 1000 mg/mL at pH 7.0[25]). This has been explained by the fact that the predominant species of PZA (>99.99%) under neutral pH conditions will be the charged POA, which is unable to cross the bacterial cell membrane.[25] In this study, we measured the pH of the dissected type I granulomas which had a pH of 7.4−7.6 within caseum, as was also shown in another recent study in C3HeB/FeJ mice.[9] Therefore, the favorable lesion penetration characteristics of PZA observed in this study may be offset by the increased MIC of PZA under higher pH conditions, which provides a potential explanation that neutral pH could be the predominant reason for the lack of efficacy for PZA in the less-responsive mouse subpopulation. However, earlier studies have shown that other in vitro conditions can confer PZA susceptibility at neutral pH, many of which are also present in necrotic lesions (such as hypoxia,[39] and nutrient starvation in stationary cultures[40]). A recent study provided more evidence to support this by demonstrating that PZA and POA susceptibility in vitro is independent of environmental pH.[41] Therefore, the reduced PZA activity in C3HeB/FeJ mice might only be explained by the contributions of the various local environmental factors combined in necrotic lesions, and not by pH alone, thereby affecting the metabolic state of bacteria in a profound and specific way. While the exact reason for the increased efficacy contributed by PZA to the low BDQ dose is not known, PZA also exhibits synergism with rifampin as well as with newer antituberculosis drugs, the spectinamides[42] in C3HeB/FeJ mice (unpublished results), which suggests that this effect may be a general phenomenon of this drug. Partnered with other drugs, PZA appears to potentiate efficacy under the same environmental conditions that prohibited PZA to act as a single agent. These data suggest that the synergistic effects of PZA with companion drugs and the bactericidal activity observed when used as a single drug may be separable mechanisms. Cooperative mechanisms of action,[11,12,23] different target subpopulations of metabolically distinct bacteria, and non-overlapping penetration characteristics (as presented in this study) may also contribute to the observed efficacy when used in combination.

Using both the approaches of mathematical modeling of PK data in conjunction with MALDI-MSI analysis, we were able to determine that while plasma exposure correlated with pulmonary lesion exposure for PZA and POA, plasma exposure levels were not an appropriate surrogate for intralesional levels of BDQ and M2 when examining caseous necrotic granulomas. MALDI-MSI analysis allowed us to clearly visualize the homogeneous distribution of PZA and POA, and the nonuniform distribution of BDQ and M2 on an individual lesion basis. This allowed us to correlate the specific histological type of granuloma with the differential drug accumulation characteristics in the lungs of a surrogate mouse model. Importantly, the C3HeB/FeJ mouse model was instrumental in identifying some potential liabilities of these compounds, which allowed us to further investigate their causes using experimental techniques, including MALDI-MSI and in vitro assays. While the majority of the studies presented here focused on treatment response following single drug administration, ongoing studies are investigating whether single drugs hampered by hypoxic environments, drug distribution across diverse lesion types, or pH conditions will be able to overcome these issues after prolonged combination treatment with other potent drugs.

As the microenvironmental conditions within caseous necrotic granulomas have been demonstrated to impact the treatment response of CFZ due to hypoxia,[7] PZA due to intragranuloma conditions including pH[9] (and this work), and now BDQ due to differential lesion-specific drug partitioning, this further supports the idea that mouse models which display more realistic pulmonary pathology have increased utility in TB drug development. Better knowledge of localized differences in intrapulmonary drug exposure and the impact of lesion heterogeneity on drug penetration and action will improve our understanding of drug efficacy and facilitate the rational combination of novel TB drugs into more effective drug regimens.

MATERIALS AND METHODS

Animals. Female specific pathogen-free BALB/c and C3HeB/FeJ mice aged 8−10 weeks were purchased from Charles River Laboratories (Wilmington, MA) and Jackson Laboratories (Bar Harbor, ME), respectively. Mice were housed in a biosafety level III animal facility and maintained with sterile bedding, water, and mouse chow. Specific pathogen-free status was verified by testing sentinel mice housed within the colony. This study was performed in strict accordance with the recommendations in the Guide for the Care and Use of Laboratory Animals of the National Institutes of Health. The animal protocols involving mice were approved by Colorado State University's Institutional Animal Care and Use Committee under protocol # 14-5262A.

Aerosol Infection. The *M. tuberculosis* Erdman strain (TMCC 107) was used for aerosol infections of mice, and the

DOI: 10.1021/acsinfecdis.5b00127
ACS Infect. Dis. 2016, 2, 251−267

inocula were prepared as previously described.[43] Briefly, the bacteria were originally grown as a pellicle to generate low passage seed lots. Working stocks were generated by growing to mid log phase in Proskauer−Beck medium containing 0.05% Tween 80 (Sigma Chemical Co., St. Louis, MO) in three passages, enumerated by colony counting on 7H11 agar plates, divided into 1.5 mL aliquots, and stored at −70 °C until use. C3HeB/FeJ mice were exposed to a LDA infection using a Glas-Col inhalation exposure system, as previously described,[44] resulting in an average of 75 bacteria in the lungs on the day of exposure. Five mice were sacrificed the following day to determine the number of CFU implanted in the lungs.

Drug Efficacy Experiments and Bacterial Enumeration. For drug efficacy experiments, BALB/c and C3HeB/FeJ mice (n = 5 per group per time point) were dosed with PZA (150 or 300 mg/kg; Sigma-Aldrich), BDQ (10 or 25 mg/kg; kind gift of Koen Andries, Janssen Pharmaceutica), or PZA and BDQ in combination (150 mg/kg, 10 mg/kg) via oral gavage five times weekly. BDQ was prepared as described before,[26] in glass vials using 20% w/v 2-hydroxypropyl-β-cyclodextrin at pH 2.0 until dissolved, filter-sterilized, and the pH adjusted to 3.5. PZA was combined with water and warmed to 50 °C to facilitate dissolution. At the time of sacrifice, whole lungs were aseptically removed and disrupted with a tissue homogenizer (Glas-Col Inc., Terre Haute, IN). The number of viable organisms was determined by plating serial dilutions of whole lungs homogenized in 4 mL of phosphate buffered saline (PBS) on Middlebrook 7H11 agar plates supplemented with oleic acid−albumin−dextrose−catalase (OADC; GIBCO BRL, Gaithersburg, MD), 0.03 mg/mL cycloheximide, and 0.05 mg/mL carbenicillin. Due to the long half-life and high protein binding capacity of BDQ, lungs and spleens from drug-treated animals were homogenized in saline plus 10% bovine serum albumin and plated on 7H11-OADC agar plates containing 0.4% activated charcoal to prevent drug carry-over as described previously.[23] For BDQ resistance enumeration, organs were plated on 7H11/OADC agar plates containing 0.5 μg/mL BDQ. Colonies were counted after at least 21 days of incubation at 37 °C and kept for 10 weeks to ensure that all viable colonies would be detected. For pH determinations, previously frozen dissected caseum (n = 3) was homogenized in 100 μL of distilled water and measured using pH paper (Fisher Scientific, Pittsburgh, PA).

Statistical Analysis. The viable CFU counts were converted to logarithms as $\log_{10}(x + 1)$, where x = total organ CFU count, which were then evaluated by a one-way analysis of variance (ANOVA) or two-way ANOVA, followed by a multiple comparison analysis of variance by a one-way Tukey's test or Dunnett's test (SAS Software program, Research Triangle Park, NC). Differences were considered significant at the 95% level of confidence. A two-way ANOVA on response type was performed separately for each drug treatment. The difference between means of the responding and less-responsive mouse subpopulations was determined to be highly significant ($P < 0.001$).

Histological Analysis. Frozen sections were fixed in 4% paraformaldehyde in PBS and stained with either hematoxylin and eosin or SYBR Gold and DAPI as described previously.[45] Briefly, slides were stained in a solution of SYBR Gold (Life Technologies, Grand Island, NY), phenol, glycerin, and isopropanol in distilled water with gentle heating, washed with acid alcohol (0.5% hydrochloric acid, 70% isopropanol) for 3 min, then washed in water, and mounted using Prolong Gold antifade (Life Technologies) mounting medium. Slides were visualized using a Nikon Intensilight mercury vapor lamp and scanned using a Nikon TE-I motorized microscope controlled by Nikon NIS Elements AR software v. 4.00.01 (Nikon, Melville, NY) with FITC, TRITC, and DAPI filters.

Pharmacokinetic Experiments. A single dose of BDQ (25 mg/kg) or PZA (150 mg/kg) was administered via oral gavage. In this study, PZA was coadministered with moxifloxacin to study the PK parameters for both drugs (moxifloxacin results not shown). Both drugs are known not to interact for the purposes of LC/MS/MS and MALDI-MSI analysis. Drug doses were individually tailored to each mouse based upon body weight on the day of dosing. For PZA, six time points using 5 BALB/c and 5 C3HeB/FeJ mice were performed at 0.08, 0.25, 0.5, 1, 2.5, and 8 h postdose. Similarly, for BDQ, nine time points (n = 5 mice) were performed at 0.5, 1, 3, 8, 24, 48, 72, 96, and 168 h postdose. Nondosed infected mice and dosed uninfected mice were prepared as controls. Nonterminal blood collections obtained via facial vein puncture occurred at 0.75, 1.5, and 5 h postdose for PZA and 2, 4, and 144 h postdose for BDQ. Whole lung samples for MALDI-MSI analysis were collected by freezing over liquid nitrogen vapor and stored at −80 °C until analysis.

Whole blood was obtained via cardiac puncture and processed in a plasma separator tube (Becton, Dickinson and Co., Franklin Lakes, NJ) centrifuged at 10,000 RCF for 2 min at 4 °C, aliquoted into Eppendorf microcentrifuge tubes, and stored at −80 °C until analysis. Whole lung samples consisting of the cranial, medial, and accessory lung lobes were collected in a preweighed, soft tissue homogenization tube (Bertin Corp., Rockville, MD). The left lobe and right caudal lobe were collected and histologically uninvolved lung tissue identified by visual inspection was collected into tissue homogenization tubes. For BALB/c mice, cellular non-necrotizing lesions (type III) were individually dissected and combined into preweighed tissue homogenization tubes for individual animals. For C3HeB/FeJ mice, encapsulated caseous necrotic granulomas (type I) were similarly collected for individual animals. Samples were stored at −80 °C until analysis.

Drug Accumulation Assay in Human THP-1 Cells. THP-1 cells (ATCC TIB-202) were initiated at a density of 2−4 × 10^5 cells/mL in 175 cm^2 flasks in RPMI 1640 medium (Corning) supplemented with 10% fetal bovine serum and 2 mM L-glutamine (Sigma, St Louis, MO). After 3 days of incubation, viable cells were counted using the trypan blue exclusion method and diluted to 6.67 × 10^5 cells/mL. Phorbol 12-myristate 13-acetate (PMA) was added to a final concentration of 100 nM, and 1 × 10^5 cells were seeded into each well of 96-well tissue culture-treated plates (Greiner Bio One, Monroe, NC). After overnight incubation, culture medium was carefully removed and media with drugs (PZA, 1 mM; POA, 0.4 mM; BDQ, 0.5 mM) were added. After 30 min incubation under ambient environment, media were removed and cells were gently washed twice with an equal volume of ice cold PBS to remove any extracellular drug residuals. Cells were lysed with an equal volume of deionized water for 1 h at 37 °C under ambient environment. Lysates were transferred to 1.5 mL centrifuge tubes and stored at −20 °C or analyzed immediately. To quantify the total number of cells/well, 100 μL of each cell lysate was added to a clear-bottom black-sided 96-well plate. 100 μL of PicoGreen (Life Technologies) was added, and the plates were mixed and incubated for 2−5 min, protected from light. Fluorescence was

DOI: 10.1021/acsinfecdis.5b00127
ACS Infect. Dis. 2016, 2, 251−267

read at 520 nm (excitation wavelength 480 nM). Samples were blank subtracted, and cell number interpolations were made from a standard curve.

Tissue Sectioning and Matrix Application. Twelve micrometer thick tissue sections were prepared using a Leica CM1850 cryostat (Buffalo Grove, IL) and thaw-mounted onto stainless steel slides (for MALDI-MSI analysis) or frosted glass microscope slides (for H&E staining). After sectioning, tissue sections were immediately transferred to a −80 °C freezer for storage. Prior to MALDI-MSI analysis, tissue sections were removed from the −80 °C freezer and allowed to reach room temperature for 15 min. 25 mg/mL 2,5-dihydroxybenzoic acid matrix (50% methanol, 0.1% trifluoroacetic acid; Sigma-Aldrich) was applied to the tissue by airspray deposition. The airbrush (Paasche Model VL, Chicago, IL) was positioned at a distance of 30 cm from the tissue, and 30 passes over the tissue were performed with the tissue being allowed to dry for 30 s between coatings.

MALDI-MSI Analysis. MALDI-MSI analysis was performed using a MALDI LTQ Orbitrap XL mass spectrometer (Thermo Fisher Scientific, Bremen, Germany) with a resolution of 60,000 [at m/z 400, full width at half-maximum (fwhm)]. The resolution was sufficient to resolve the drug and respective metabolite peaks from background without the requirement for MS/MS and subsequent loss of signal. However, drug peak identities were confirmed by acquiring several MS/MS spectra directly from dosed lung tissue sections. Standards of BDQ and PZA were analyzed both direct from the stainless steel target plate and spiked into control rat lung tissue to optimize instrument parameters.

For BDQ analysis, spectra were acquired in positive ion mode with a mass window of m/z 100−600. This range covered both BDQ and its major metabolite *N*-desmethyl-BDQ (M2). A laser energy of 10 μJ was applied, and 50 laser shots were fired at each position (total of 1 microscan per position). The laser step size was set to 75 μm. For PZA and pyrazinoic acid (POA) analysis, spectra were acquired in positive mode with a mass window of m/z 75−500. A laser energy of 7.5 μJ was applied, and 50 laser shots were fired at each position (total of 1 microscan per position). The laser step size was set to 75 μm. Total acquisition times ranged between 5 and 12 h. The limits of detection (LOD) were determined as follows. Standards were spotted on human or mouse drug-naive tissue (3 mm diameter circles), and the weight of the underlying tissue (7.07 mm^2) was estimated at 0.042 mg, using the measured average weight of a 1 cm × 1.5 cm × 12 μm section piece as 0.9 mg. The LOD was assessed from signals detected on spotted standards on granuloma and uninvolved lung sections following matrix application by airspray. The LOD were 1 pmol or 3 μg/g for PZA and 1.2 μg/g for BDQ.

Data visualization was performed using Thermo ImageQuest software. Normalized ion images of BDQ were generated by normalizing BDQ $[M + H]^+$ signal (m/z 555.164 ± 0.003) and M2 $[M + H]^+$ signal (m/z 541.148 ± 0.003) to the total ion current (TIC). Normalized ion images of PZA $[M + 2H]^+$ (m/z 125.058 ± 0.003) and POA $[M + 2H]^+$ (m/z 126.042 ± 0.003) were generated by normalizing their signal to the TIC. Extracted ion images were interpolated using the linear interpolate function.

Drug Quantitation by HPLC Coupled to Tandem Mass Spectrometry (LC/MS/MS). Individual lung granulomas and pieces of uninvolved lung tissue were weighed and homogenized in approximately—but accurately recorded—5 volumes of PBS. Homogenization was achieved using a FastPrep-24 instrument (MP Biomedicals) and 1.4 mm zirconium oxide beads (Bertin Corp.). Proteins were precipitated by adding 9 volumes of 1:1 acetonitrile:methanol containing 0.5 mg/mL of verapamil (for BDQ), pyrazinamide-^{15}N,D3 or pyrazinecarboxylic acid-D3 (Toronto Research Chemicals, Inc.) as internal standards to 1 volume of plasma or homogenized tissue sample. The mixtures were vortexed for 5 min and centrifuged at 4,000 rpm for 5 min. The supernatant was then transferred for LC/MS/MS analysis.

High-pressure liquid chromatography (HPLC) coupled to tandem mass spectrometry (LC/MS/MS) analysis was performed on a Sciex Applied Biosystems Qtrap 4000 triple-quadrupole mass spectrometer coupled to an Agilent 1260 HPLC system to quantify the clinical samples. PZA and POA chromatography was performed with an Agilent Zorbax SB-C8 column (4.6 × 75 mm; particle size, 3.5 μm) using a reverse phase gradient elution. BDQ chromatography was performed on an Agilent SB-C8 column (2.1 × 30 mm; particle size, 3.5 μm) using a reverse phase gradient elution. All gradients used 0.1% formic acid in Milli-Q deionized water for the aqueous mobile phase and 0.1% formic acid in acetonitrile for the organic mobile phase. Multiple-reaction monitoring of parent/daughter transitions in electrospray positive-ionization mode was used to quantify the analytes. Sample analysis was accepted if the concentrations of the quality control samples were within 20% of the nominal concentration. Data processing was performed using Analyst software (version 1.6.2; Applied Biosystems Sciex).

Neat 1 mg/mL DMSO stocks of all compounds were serially diluted in 50/50 acetonitrile/H_2O to create standard curves and quality control spiking solutions. 20 μL of neat spiking solutions was added to 20 μL of drug free plasma or control tissue homogenate, and extraction was performed by adding 180 μL of acetonitrile/methanol (50/50) protein precipitation solvent containing the internal standards. Extracts were vortexed for 5 min and centrifuged at 4000 rpm for 5 min. The supernatant was transferred for HPLC-MS/MS analysis. Human control plasma from BioreclamationIVT (K2-EDTA) was used to build standard curves. Gamma irradiated uninvolved lung, lesion, and caseum from tuberculosis-infected New Zealand White rabbits were used as surrogate matrix to build standard curves. Surrogate matrices were homogenized by adding 4 parts PBS buffer:1 part surrogate tissue. The tissues were homogenized using a SPEX Sample Prep Geno/Grinder 2010 for 5 min at 1500 rpm. The labeled internal standards were sourced from Toronto Research Chemicals. Respectively for BDQ, PZA, and POA the internal standards were verapamil, PZA-^{15}N-D3, and POA-D3. The following MRM transitions were used: BDQ (555.20/58.20), PZA (124/81.1), POA (125.2/81.1).

Pharmacokinetic Data Analysis. A PK data analysis of PZA and its major metabolite POA of concentration−time measurements following a single 150 mg/kg oral dose of PZA in TB-infected mouse plasma and lung tissue samples was performed using noncompartmental and empirical compartmental methods.[46] A similar analysis was performed for BDQ (25 mg/kg single dose) and its M2 metabolite. The lung tissue samples included whole lung, and dissected uninvolved lung and lesion samples.

Noncompartmental Analysis. A noncompartmental analysis was performed on the mean BDQ and M2 plasma and lung tissue concentrations at each sampled time point. The

DOI: 10.1021/acsinfecdis.5b00127
ACS Infect. Dis. 2016, 2, 251−267

PK parameters obtained were maximum concentration (C_{max}) and corresponding time (t_{max}), area under the concentration−time curve from time of dose administration to the last sampled time point at t = 8 h (AUC_{8h}) for PZA/POA and t = 168 h (AUC_{168h}) for BDQ/M2, and the terminal elimination half-life ($t_{1/2}$).

Compartmental Analysis. An empirical compartmental analysis of the individual plasma and lung tissue concentrations of PZA, POA, BDQ, and M2 in BALB/c and C3HeB/FeJ mice was performed to obtain population distributions of PK parameters descriptive of absorption, clearance, volume of distribution, tissue:plasma partition coefficients, and lung tissue penetration rates. The compartmental model structure and parametrization were based on previously described models for plasma, lung, and lesion PK in TB-infected rabbits by Kjellsson et al.,[29] and plasma BDQ and metabolite PK in humans by Svensson et al.[30] Parameter estimation was performed using a Bayesian population analysis[47] with posterior distributions sampled using Markov chain Monte Carlo (MCMC) simulation.

Monte Carlo Simulation. A 10,000 iteration Monte Carlo (MC) simulation of plasma and tissue concentration−time profiles following a single 150 mg/kg PZA dose or a 25 mg/kg BDQ dose was run using the compartmental model and posterior population parameters. Each model parameter was sampled from a log-normal distribution specified by the corresponding marginal posterior geometric mean GM, geometric standard deviation GSD, with bounds $GM \cdot e^{\pm 3 \cdot \ln(GSD)}$. Body weights were sampled from a normal distribution specified by the experimentally measured mean and SD and bounded by the observed minimum and maximum values.

Computational Software. R v3.1.2[48] was used for statistical calculations, including the noncompartmental analysis. MCSim v5.5.0[49] was used for PK−PD model simulations, including MCMC and MC simulations.

■ ASSOCIATED CONTENT

Supporting Information

The Supporting Information is available free of charge on the ACS Publications website at DOI: 10.1021/acsinfecdis.5b00127.

Summary statistics of compartmental model parameter distributions, PZA and BDQ activity plots, BDQ and M2 compartmental structure, and MC simulations (PDF)

■ AUTHOR INFORMATION

Corresponding Author

*Phone: 970-491-3079. Fax 970-491-1815. E-mail: Anne.Lenaerts@colostate.edu.

Notes

The authors declare the following competing financial interest(s): K.A. is an employee of Janssen Pharmaceutica, the company that developed bedaquiline.

■ ACKNOWLEDGMENTS

This work was supported by the Bill and Melinda Gates Foundation under Grant ID numbers 1033596, "Evaluation of a New Murine Model for Testing Tuberculosis Chemotherapy" to A.J.L.; 1037174, "Qualification of C3HeB/FeJ mice for Experimental Chemotherapy of Tuberculosis" to E.L.N.; and 1066499, "Integrated Pharmacokinetics to Rationally Design New Drug Combinations for TB" to V.D. We thank Omar Vandal and Khisimuzi Mdluli for their helpful discussions. We acknowledge the staff of the Laboratory Animal Resources at Colorado State University for their animal care.

■ REFERENCES

(1) Canetti, G. (1955) *The tubercle bacillus in the pulmonary lesion of man; histobacteriology and its bearing on the therapy of pulmonary tuberculosis*, American rev. ed., Springer Publishing Co., New York, NY.

(2) Hunter, R. L., Actor, J. K., Hwang, S. A., Karev, V., and Jagannath, C. (2014) Pathogenesis of post primary tuberculosis: immunity and hypersensitivity in the development of cavities. *Ann. Clin. Lab. Sci. 44*, 365−387.

(3) Lenaerts, A., Barry, C. E., 3rd, and Dartois, V. (2015) Heterogeneity in tuberculosis pathology, microenvironments and therapeutic responses. *Immunol Rev. 264*, 288−307.

(4) Bumann, D. (2015) Heterogeneous host-pathogen encounters: act locally, think globally. *Cell Host Microbe 17*, 13−19.

(5) Driver, E. R., Ryan, G. J., Hoff, D. R., Irwin, S. M., Basaraba, R. J., Kramnik, I., and Lenaerts, A. J. (2012) Evaluation of a mouse model of necrotic granuloma formation using C3HeB/FeJ mice for testing of drugs against *Mycobacterium tuberculosis*. *Antimicrob. Agents Chemother. 56*, 3181−3195.

(6) Irwin, S. M., Driver, E., Lyon, E., Schrupp, C., Ryan, G., Gonzalez-Juarrero, M., Basaraba, R. J., Nuermberger, E. L., and Lenaerts, A. J. (2015) Presence of multiple lesion types with vastly different microenvironments in C3HeB/FeJ mice following aerosol infection with *Mycobacterium tuberculosis*. *Dis. Models & Mech. 8*, 591−602.

(7) Irwin, S. M., Gruppo, V., Brooks, E., Gilliland, J., Scherman, M., Reichlen, M. J., Leistikow, R., Kramnik, I., Nuermberger, E. L., Voskuil, M. I., and Lenaerts, A. J. (2014) Limited activity of clofazimine as a single drug in a mouse model of tuberculosis exhibiting caseous necrotic granulomas. *Antimicrob. Agents Chemother. 58*, 4026−4034.

(8) Yano, T., Kassovska-Bratinova, S., Teh, J. S., Winkler, J., Sullivan, K., Isaacs, A., Schechter, N. M., and Rubin, H. (2011) Reduction of clofazimine by mycobacterial type 2 NADH:quinone oxidoreductase: a pathway for the generation of bactericidal levels of reactive oxygen species. *J. Biol. Chem. 286*, 10276−10287.

(9) Lanoix, J. P., Lenaerts, A. J., and Nuermberger, E. L. (2015) Heterogeneous disease progression and treatment response in a C3HeB/FeJ mouse model of tuberculosis. *Dis. Models & Mech. 8*, 603−610.

(10) Koul, A., Vranckx, L., Dendouga, N., Balemans, W., Van den Wyngaert, I., Vergauwen, K., Gohlmann, H. W., Willebrords, R., Poncelet, A., Guillemont, J., Bald, D., and Andries, K. (2008) Diarylquinolines are bactericidal for dormant mycobacteria as a result of disturbed ATP homeostasis. *J. Biol. Chem. 283*, 25273−25280.

(11) Veziris, N., Ibrahim, M., Lounis, N., Andries, K., and Jarlier, V. (2011) Sterilizing activity of second-line regimens containing TMC207 in a murine model of tuberculosis. *PLoS One 6*, e17556.

(12) Williams, K., Minkowski, A., Amoabeng, O., Peloquin, C. A., Taylor, D., Andries, K., Wallis, R. S., Mdluli, K. E., and Nuermberger, E. L. (2012) Sterilizing activities of novel combinations lacking first- and second-line drugs in a murine model of tuberculosis. *Antimicrob. Agents Chemother. 56*, 3114−3120.

(13) Diacon, A. H., Donald, P. R., Pym, A., Grobusch, M., Patientia, R. F., Mahanyele, R., Bantubani, N., Narasimooloo, R., De Marez, T., van Heeswijk, R., Lounis, N., Meyvisch, P., Andries, K., and McNeeley, D. F. (2012) Randomized pilot trial of eight weeks of bedaquiline (TMC207) treatment for multidrug-resistant tuberculosis: long-term outcome, tolerability, and effect on emergence of drug resistance. *Antimicrob. Agents Chemother. 56*, 3271−3276.

(14) Diacon, A. H., Pym, A., Grobusch, M., Patientia, R., Rustomjee, R., Page-Shipp, L., Pistorius, C., Krause, R., Bogoshi, M., Churchyard, G., Venter, A., Allen, J., Palomino, J. C., De Marez, T., van Heeswijk, R. P., Lounis, N., Meyvisch, P., Verbeeck, J., Parys, W., de Beule, K., Andries, K., and Mc Neeley, D. F. (2009) The diarylquinoline

DOI: 10.1021/acsinfecdis.5b00127
ACS Infect. Dis. 2016, 2, 251−267

TMC207 for multidrug-resistant tuberculosis. *N. Engl. J. Med. 360*, 2397−2405.
(15) Anonymous (1981) Controlled trial of four thrice-weekly regimens and a daily regimen all given for 6 months for pulmonary tuberculosis. *Lancet 317*, 171−174.
(16) Combs, D. L., O'Brien, R. J., and Geiter, L. J. (1990) USPHS Tuberculosis Short-Course Chemotherapy Trial 21: effectiveness, toxicity, and acceptability. The report of final results. *Ann. Intern. Med. 112*, 397−406.
(17) Ahmad, Z., Fraig, M. M., Bisson, G. P., Nuermberger, E. L., Grosset, J. H., and Karakousis, P. C. (2011) Dose-dependent activity of pyrazinamide in animal models of intracellular and extracellular tuberculosis infections. *Antimicrob. Agents Chemother. 55*, 1527−1532.
(18) Ibrahim, M., Andries, K., Lounis, N., Chauffour, A., Truffot-Pernot, C., Jarlier, V., and Veziris, N. (2007) Synergistic activity of R207910 combined with pyrazinamide against murine tuberculosis. *Antimicrob. Agents Chemother. 51*, 1011−1015.
(19) Diacon, A. H., Dawson, R., von Groote-Bidlingmaier, F., Symons, G., Venter, A., Donald, P. R., van Niekerk, C., Everitt, D., Winter, H., Becker, P., Mendel, C. M., and Spigelman, M. K. (2012) 14-day bactericidal activity of PA-824, bedaquiline, pyrazinamide, and moxifloxacin combinations: a randomised trial. *Lancet 380*, 986−993.
(20) Zhang, Y., Wade, M. M., Scorpio, A., Zhang, H., and Sun, Z. (2003) Mode of action of pyrazinamide: disruption of *Mycobacterium tuberculosis* membrane transport and energetics by pyrazinoic acid. *J. Antimicrob. Chemother. 52*, 790−795.
(21) Shi, W., Zhang, X., Jiang, X., Yuan, H., Lee, J. S., Barry, C. E., 3rd, Wang, H., Zhang, W., and Zhang, Y. (2011) Pyrazinamide inhibits trans-translation in *Mycobacterium tuberculosis*. *Science 333*, 1630−1632.
(22) Zhang, S., Chen, J. Z., Shi, W. L., Liu, W., Zhang, W. H., and Zhang, Y. (2013) Mutations in panD encoding aspartate decarboxylase are associated with pyrazinamide resistance in *Mycobacterium tuberculosis*. *Emerging Microbes Infect. 2*, e34.
(23) Tasneen, R., Li, S. Y., Peloquin, C. A., Taylor, D., Williams, K. N., Andries, K., Mdluli, K. E., and Nuermberger, E. L. (2011) Sterilizing activity of novel TMC207- and PA-824-containing regimens in a murine model of tuberculosis. *Antimicrob. Agents Chemother. 55*, 5485−5492.
(24) Global Alliance for Tuberculosis Drug Development. A Phase 2 Open Label Partially Randomized Trial to Evaluate the Efficacy, Safety and Tolerability of Combinations of Bedaquiline, Moxifloxacin, PA-824 and Pyrazinamide in Adult Subjects With Drug-Sensitive or Multi Drug-Resistant Pulmonary Tuberculosis. (NC-005), in *ClinicalTrials.gov*. https://clinicaltrials.gov/ct2/show/NCT02193776?term=nc-005&rank=1, Bethesda, MD.
(25) Zhang, Y., Permar, S., and Sun, Z. (2002) Conditions that may affect the results of susceptibility testing of *Mycobacterium tuberculosis* to pyrazinamide. *J. Med. Microbiol. 51*, 42−49.
(26) Rouan, M. C., Lounis, N., Gevers, T., Dillen, L., Gilissen, R., Raoof, A., and Andries, K. (2012) Pharmacokinetics and pharmacodynamics of TMC207 and its N-desmethyl metabolite in a murine model of tuberculosis. *Antimicrob. Agents Chemother. 56*, 1444−1451.
(27) Ahmad, Z., Nuermberger, E. L., Tasneen, R., Pinn, M. L., Williams, K. N., Peloquin, C. A., Grosset, J. H., and Karakousis, P. C. (2010) Comparison of the 'Denver regimen' against acute tuberculosis in the mouse and guinea pig. *J. Antimicrob. Chemother. 65*, 729−734.
(28) Via, L. E., Savic, R., Weiner, D. M., Zimmerman, M. D., Prideaux, B., Irwin, S. M., Lyon, E., O'Brien, P., Gopal, P., Eum, S., Lee, M., Lanoix, J. P., Dutta, N. K., Shim, T., Cho, J. S., Kim, W., Karakousis, P. C., Lenaerts, A., Nuermberger, E., Barry, C. E., 3rd, and Dartois, V. (2015) Host-Mediated Bioactivation of Pyrazinamide: Implications for Efficacy, Resistance, and Therapeutic Alternatives. *ACS Infect. Dis. 1*, 203−214.
(29) Kjellsson, M. C., Via, L. E., Goh, A., Weiner, D., Low, K. M., Kern, S., Pillai, G., Barry, C. E., 3rd, and Dartois, V. (2012) Pharmacokinetic evaluation of the penetration of antituberculosis agents in rabbit pulmonary lesions. *Antimicrob. Agents Chemother. 56*, 446−457.
(30) Svensson, E. M., Aweeka, F., Park, J. G., Marzan, F., Dooley, K. E., and Karlsson, M. O. (2013) Model-based estimates of the effects of efavirenz on bedaquiline pharmacokinetics and suggested dose adjustments for patients coinfected with HIV and tuberculosis. *Antimicrob. Agents Chemother. 57*, 2780−2787.
(31) Prideaux, B., and Stoeckli, M. (2012) Mass spectrometry imaging for drug distribution studies. *J. Proteomics 75*, 4999−5013.
(32) Dartois, V. (2014) The path of anti-tuberculosis drugs: from blood to lesions to mycobacterial cells. *Nat. Rev. Microbiol. 12*, 159−167.
(33) Prideaux, B., Dartois, V., Staab, D., Weiner, D. M., Goh, A., Via, L. E., Barry, C. E., 3rd, and Stoeckli, M. (2011) High-sensitivity MALDI-MRM-MS imaging of moxifloxacin distribution in tuberculosis-infected rabbit lungs and granulomatous lesions. *Anal. Chem. 83*, 2112−2118.
(34) Dhillon, J., Andries, K., Phillips, P. P., and Mitchison, D. A. (2010) Bactericidal activity of the diarylquinoline TMC207 against *Mycobacterium tuberculosis* outside and within cells. *Tuberculosis (Oxford, U. K.) 90*, 301−305.
(35) Baik, J., Stringer, K. A., Mane, G., and Rosania, G. R. (2013) Multiscale distribution and bioaccumulation analysis of clofazimine reveals a massive immune system-mediated xenobiotic sequestration response. *Antimicrob. Agents Chemother. 57*, 1218−1230.
(36) Barry, V. C., Belton, J. G., Conalty, M. L., Denneny, J. M., Edward, D. W., O'Sullivan, J. F., Twomey, D., and Winder, F. (1957) A new series of phenazines (rimino-compounds) with high antituberculosis activity. *Nature 179*, 1013−1015.
(37) Prideaux, B., Via, L. E., Zimmerman, M. D., Eum, S., Sarathy, J., O'Brien, P., Chen, C., Kaya, F., Weiner, D. M., Chen, P. Y., Song, T., Lee, M., Shim, T. S., Cho, J. S., Kim, W., Cho, S. N., Olivier, K. N., Barry, C. E., 3rd, and Dartois, V. (2015) The association between sterilizing activity and drug distribution into tuberculosis lesions. *Nat. Med. 21*, 1223−1227.
(38) Zhang, Y., and Mitchison, D. (2003) The curious characteristics of pyrazinamide: a review. *Int. J. Tuberc. Lung Dis. 7*, 6−21.
(39) Cho, S. H., Warit, S., Wan, B., Hwang, C. H., Pauli, G. F., and Franzblau, S. G. (2007) Low-oxygen-recovery assay for high-throughput screening of compounds against nonreplicating Mycobacterium tuberculosis. *Antimicrob. Agents Chemother. 51*, 1380−1385.
(40) Hu, Y., Coates, A. R., and Mitchison, D. A. (2006) Sterilising action of pyrazinamide in models of dormant and rifampicin-tolerant Mycobacterium tuberculosis. *Int. J. Tuberc. Lung Dis. 10*, 317−322.
(41) Peterson, N. D., Rosen, B. C., Dillon, N. A., and Baughn, A. D. (2015) Uncoupling Environmental pH and Intrabacterial Acidification from Pyrazinamide Susceptibility in Mycobacterium tuberculosis. *Antimicrob. Agents Chemother. 59*, 7320−7326.
(42) Lee, R. E., Hurdle, J. G., Liu, J., Bruhn, D. F., Matt, T., Scherman, M. S., Vaddady, P. K., Zheng, Z., Qi, J., Akbergenov, R., Das, S., Madhura, D. B., Rathi, C., Trivedi, A., Villellas, C., Lee, R. B., Rakesh, Waidyarachchi, S. L., Sun, D., McNeil, M. R., Ainsa, J. A., Boshoff, H. I., Gonzalez-Juarrero, M., Meibohm, B., Bottger, E. C., and Lenaerts, A. J. (2014) Spectinamides: a new class of semisynthetic antituberculosis agents that overcome native drug efflux. *Nat. Med. 20*, 152−158.
(43) Lenaerts, A. J., Gruppo, V., Marietta, K. S., Johnson, C. M., Driscoll, D. K., Tompkins, N. M., Rose, J. D., Reynolds, R. C., and Orme, I. M. (2005) Preclinical testing of the nitroimidazopyran PA-824 for activity against *Mycobacterium tuberculosis* in a series of in vitro and in vivo models. *Antimicrob. Agents Chemother. 49*, 2294−2301.
(44) Kelly, B. P., Furney, S. K., Jessen, M. T., and Orme, I. M. (1996) Low-dose aerosol infection model for testing drugs for efficacy against *Mycobacterium tuberculosis*. *Antimicrob. Agents Chemother. 40*, 2809−2812.
(45) Ryan, G. J., Shapiro, H. M., and Lenaerts, A. J. (2014) Improving acid-fast fluorescent staining for the detection of mycobacteria using a new nucleic acid staining approach. *Tuberculosis (Oxford, U. K.) 94*, 511−518.

DOI: 10.1021/acsinfecdis.5b00127
ACS Infect. Dis. 2016, 2, 251−267

(46) Gabrielsson, J., and Weiner, D. (2007) *Pharmacokinetic and pharmacodynamic data analysis: concepts and applications*, 4th ed., Swedish Pharmaceutical Press, Stockholm, Sweden.
(47) Bernillon, P., and Bois, F. Y. (2000) Statistical issues in toxicokinetic modeling: a bayesian perspective. *Environ. Health Perspect 108* (Suppl. 5), 883−893.
(48) R. Core Team (2014) *R: A Language and Environment for Statistical Computing* (R Foundation for Statistical Computing, Ed.) Vienna, Austria.
(49) Bois, F. Y. (2009) GNU MCSim: Bayesian statistical inference for SBML-coded systems biology models. *Bioinformatics 25*, 1453−1454.

DOI: 10.1021/acsinfecdis.5b00127
ACS Infect. Dis. 2016, 2, 251−267